Cathepsin S Causes Inflammatory Pain *via* Biased Agonism of PAR2 and TRPV4*

Peishen Zhao[‡1], TinaMarie Lieu[‡1], Nicholas Barlow[‡1], Matthew Metcalf[‡], Nicholas A. Veldhuis[‡], Dane D. Jensen[‡], Martina Kocan[‡], Silvia Sostegni[§], Silke Haerteis[§], Vera Baraznenok[¶], Ian Henderson[¶], Erik Lindström[¶], Raquel Guerrero-Alba[‖], Eduardo E. Valdez-Morales[‖], Wolfgang Liedtke[**], Peter McIntyre[‡‡], Stephen J. Vanner[‖], Christoph Korbmacher[§], and Nigel W. Bunnett[‡§§¶¶2]

From the [‡]Monash Institute of Pharmaceutical Sciences, Parkville 3052, Australia, [§]Institut für Zelluläre und Molekulare Physiologie, Friedrich-Alexander-Universität Erlangen-Nürnberg, 91054 Erlangen, Germany, [¶]Medivir AB, 141 Huddinge, Sweden, [‖]Gastrointestinal Diseases Research Unit, Division of Gastroenterology, Queen's University, Kingston, Ontario N7L 3N6, Canada, [**]Division of Neurology, Department of Medicine, Duke University, Durham, North Carolina 27710, [‡‡]School of Medical Sciences and Health Innovations Research Institute, RMIT University, Bundoora 3083, Australia, [§§]Department of Pharmacology, University of Melbourne, Melbourne 3010, Australia, and [¶¶]ARC Centre of Excellence in Convergent Bio-Nano Science and Technology, Monash University, Parkville 3052, Australia

Background: Proteases trigger inflammation and pain by cleaving protease-activated receptors (PARs) at defined sites.
Results: Cathepsin S (Cat-S) cleaved PAR2 at a unique site $E^{56} \downarrow T^{57}$, leading to Gαs-mediated cAMP accumulation and TRPV4-dependent inflammation and pain.
Conclusion: Cat-S is a biased agonist of PAR2- and TRPV4-dependent inflammation and pain.
Significance: PARs integrate responses to diverse proteases.

Serine proteases such as trypsin and mast cell tryptase cleave protease-activated receptor-2 (PAR2) at $R^{36} \downarrow S^{37}$ and reveal a tethered ligand that excites nociceptors, causing neurogenic inflammation and pain. Whether proteases that cleave PAR2 at distinct sites are biased agonists that also induce inflammation and pain is unexplored. Cathepsin S (Cat-S) is a lysosomal cysteine protease of antigen-presenting cells that is secreted during inflammation and which retains activity at extracellular pH. We observed that Cat-S cleaved PAR2 at $E^{56} \downarrow T^{57}$, which removed the canonical tethered ligand and prevented trypsin activation. In HEK and KNRK cell lines and in nociceptive neurons of mouse dorsal root ganglia, Cat-S and a decapeptide mimicking the Cat-S-revealed tethered ligand-stimulated PAR2 coupling to Gαs and formation of cAMP. In contrast to trypsin, Cat-S did not mobilize intracellular Ca^{2+}, activate ERK1/2, recruit β-arrestins, or induce PAR2 endocytosis. Cat-S caused PAR2-dependent activation of transient receptor potential vanilloid 4 (TRPV4) in *Xenopus laevis* oocytes, HEK cells and nociceptive neurons, and stimulated neuronal hyperexcitability by adenylyl cyclase and protein kinase A-dependent mechanisms. Intraplantar injection of Cat-S caused inflammation and hyperalgesia in mice that was attenuated by PAR2 or TRPV4 deletion and adenylyl cyclase inhibition. Cat-S and PAR2 antagonists suppressed formalin-induced inflammation and pain, which implicates endogenous Cat-S and PAR2 in inflammatory pain. Our results identify Cat-S as a biased agonist of PAR2 that causes PAR2- and TRPV4-dependent inflammation and pain. They expand the role of PAR2 as a mediator of protease-driven inflammatory pain.

Cathepsin S (Cat-S)[3] in lysosomes of macrophages, microglial cells, B-lymphocytes, and dendritic cells contributes to antigen presentation and adaptive immunity (1). Inflammatory mediators also stimulate secretion of Cat-S from macrophages and microglial cells (2, 3), and increased Cat-S activity has been detected in inflamed tissues, including synovial fluid from patients with rheumatoid arthritis (4) and colonic secretions from mice with colitis (5). Since Cat-S retains activity at neutral pH (3), the secreted protease may contribute to disease processes, including pain and inflammation. Indeed, nerve injury leads to up-regulation of Cat-S in macrophages of dorsal root ganglia (DRG) (6) and in microglial cells of the spinal cord (7). The peripheral or central administration of Cat-S causes allodynia and hyperalgesia, and Cat-S inhibition or deletion attenuates neuropathic and inflammatory pain in rodents (5–7). In the spinal cord, Cat-S induces pain by an indirect mechanism: Cat-S released from microglial cells liberates membrane-tethered fractalkine from neurons, which activates CX3CR1 on microglial cells to trigger inflammatory signals that contribute to central sensitization of pain (1, 7, 8). The mechanisms by which Cat-S in the periphery causes pain and inflammation are unknown, and whether Cat-S can directly regulate neurons *via* specific receptors has not been studied.

[3] The abbreviations used are: Cat-S, cathepsin S; PAR2, protease-activated receptor 2; DRG, dorsal root ganglia; GPCR, G protein-coupled receptor; TRP, transient receptor potential; ERK, extracellular signal-regulated kinase; MMP-1, matrix metalloprotease-1; APC, activated protein C; AP, activating peptide; BRET, bioluminescence resonance energy transfer.

Cathepsin S Biased Agonism of PAR₂

We investigated whether Cat-S causes pain by cleaving protease-activated receptor-2 (PAR_2), which is expressed by keratinocytes (9) and nociceptive neurons (10). PAR_2 is a member of a family of four G-protein coupled receptors (GPCRs) with a unique mechanism of activation: proteases cleave within the extracellular N-terminal domains of PARs to reveal tethered ligands that bind to and activate the cleaved receptors (11). Trypsin cleaves human PAR_2 at $R^{36} \downarrow S^{37}$ to expose the tethered ligand $^{37}SLIGKV$, and synthetic peptides that mimic this domain can directly activate the receptor (12, 13). Any protease that cleaves at this canonical site would be expected to trigger the same signaling events and patho-physiological outcome. Serine proteases that activate PAR_2 include trypsin I/II (12, 13), trypsin IV (14, 15), tryptase (16, 17), coagulation factors VIIa and Xa (18), acrosin (19), granzyme A (20), membrane-type serine protease 1 or matriptase (21), TMPRSS2 (22), and kallikrein 2, 4, 5, 6, and 14 (23–26). During injury and inflammation, these proteases can activate PAR_2 on nociceptive neurons to stimulate Ca^{2+}-dependent release of neuropeptides that cause neurogenic inflammation (10). PAR_2 can also sensitize transient receptor potential (TRP) ion channels, including TRP vanilloid 1 (TRPV1) (27), TRPV4 (28–30), and TRP ankyrin A1 (TRPA1) (31), leading to the release of neuropeptides in the dorsal horn of the spinal cord that induce pain transmission (32). Besides proteases that cleave the receptor at the canonical site, certain proteases cleave PAR_2 at distinct sites to destroy or remove the tethered ligand domain. These cleavage events disarm the receptor by rendering it unable to respond to activating proteases. For example, elastase cleaves PAR_2 at $S^{68} \downarrow V^{69}$, which removes the tethered ligand and thereby prevents trypsin-stimulated PAR_2 signaling (33, 34). However, the patho-physiological relevance of this PAR_2 disarming mechanism is uncertain.

We report that Cat-S, like elastase, cleaves PAR_2 distal to the canonical trypsin site. Cleavage exposes a unique tethered ligand domain that induces distinct signaling events that sensitize TRPV4 and cause hyperexcitability of nociceptive neurons, which induce neurogenic inflammation and pain. This mechanism of biased agonism of GPCRs can explain how different endogenous ligands or drugs that interact with the same GPCR can activate divergent signaling pathways with unique outcomes (35). Proteases that cleave PARs at different sites may also act as biased agonists. Elastase cleavage of PAR_2 at $S^{68} \downarrow V^{69}$ induces PAR_2-dependent activation of extracellular signal regulated kinases 1/2 (ERK1/2) by a Rho-kinase dependent pathway (34) that is distinct from trypsin-induced MAPK activation that is mediated by β-arrestins (36). Potential biased agonists of PAR_1 include elastase (37), matrix metalloprotease-1 (MMP-1) (38–40), and activated protein C (APC) (41, 42). However, although biased agonism is emerging as potential mechanism of PAR activation, the patho-physiological relevance of biased agonism is not fully understood, and nothing is known about the contribution of biased agonism for protease-induced inflammation and pain.

EXPERIMENTAL PROCEDURES

Animals—The Animal Ethics Committee of Monash University and Queen's University approved procedures using mice. C57BL/6 mice, $par_2^{-/-}$ and $par_2^{+/+}$ littermates (43) and $trpv4^{+/+}$ and $trpv4^{-/-}$ littermates (44) (8–12 weeks, male) were studied. Mice were maintained under temperature- ($22 \pm 4\,°C$) and light- (12-h light/dark cycle) controlled conditions with free access to food and water. Oocytes were collected from *Xenopus laevis* as described (45) and with approval of the animal welfare officer for the University of Erlangen-Nürnberg.

Materials—2-Furoyl-LIGRLO-NH₂ and peptides corresponding to sequences of human PAR_2 were from American Peptide Company, Inc. The Cat-S inhibitor MV026031 was from Medivir AB. MV026031 K_i values are human Cat-S 47 nM, mouse Cat-S 22 nM, human Cat-K 410 nM, mouse Cat K 4,200 nM, human Cat-B and Cat-H >200,000 nM, human Cat-L 7,800 nM, and human Cat-V 2,600 nM. The PAR_2 antagonist GB88 was a gift from the Ferring Research Institute. Anti-HA antibody was from Roche Applied Science. Monoclonal mouse antibody against FLAG sequence (DYKDDDDK) was generated by CSIRO. Goat anti-rat and anti-mouse IgG conjugated to Alexa Fluor 488 or 597 were from Invitrogen. Alpha Screen ERK1/2 activity kit was from PerkinElmer Life Sciences. Fluorogenic substrate for Cat-S (Acetyl-KQKLR-AMC) was from Bachem AG. Unless otherwise indicated, other reagents were from Sigma-Aldrich.

Recombinant Human Cat-S—Human pro-Cat-S with a hexa-histidine tag was expressed in SF9 cells using a recombinant baculovirus. Medium was collected 3 days after infection, cleared by centrifugation ($8000 \times g$, 1 h, 4 °C) and filtration (0.22 μm), and pro-Cat-S was purified by affinity chromatography over a 5-ml HiTrap Chelating HP column (GE Healthcare), charged with 0.2 M cobalt sulfate. Pro-Cat-S was eluted in 0–0.15 M gradient of imidazole in buffer S (PBS, pH 7.4–7.5, supplemented with 0.36 M NaCl, 10% glycerol, and 0.2 mM PMSF). Pro-Cat-S was dialyzed overnight against buffer S, containing 2 mM EDTA. Pro-Cat-S was activated by incubation in activation buffer (NaOAc 0.1 M, NaCl 0.1 M, EDTA 5 mM, DTT 1 mM, pH 4.5) at 37 °C for 15 to 30 min (determined by measuring the time to peak activity). Cat-S was then buffer-exchanged into PBS (pH 7.4) using an Econo-Pac 10DG column (Bio-Rad). The active site concentration of Cat-S was determined by titration with E-64 (3-carboxy-trans-2,3-epoxypropyl-leucylamido(4-guanidino)butane) in a buffer of 0.1 M Na phosphate, 0.1 M NaCl, 0.1% PEG-4000, 1 mM DTT, pH 6.5 using 100 μM boc-Val-Leu-Lys-AMC (Bachem) as substrate. Fluorescence was measured at 390 nm excitation and 460 nm emission.

Generation of cDNA Constructs, Transfections, and Cell Culture—Human PAR_2 cDNA with N-terminal Flag and C-terminal HA11 epitopes has been described (46). The Cat-S cleavage site of human PAR_2 was mutated using QuickChange II Site-directed Mutagenesis Kit (Agilent Technologies). The primers were: g184a_t185g_g187c_a188c_c191a-sense: 5′-gca cat ccc acg tca ctg gaa aag gag tta caa gtc caa aag tct ttt ctg tgg atg agt ttt-3′; antisense: 5′-aaa act cat cca cag aaa aga ctt ttg gac ttg taa ctc ctt ttc cag tga cgt ggg atg tgc-3′. Human embryonic kidney (HEK) 293 and KNRK (rat sarcoma virus transformed kidney epithelial) cells were maintained in DMEM with 10% fetal bovine serum (FBS) and 1% penicillin and streptomycin. Generation and maintenance of HEK293 and KNRK cells stably expressing human PAR_2 constructs has been described (12, 36,

46, 47). HEK293 and KNRK cells were transiently transfected with PAR$_2$ constructs as described (29, 36). Cells were co-transfected with PAR$_2$ constructs and GFP to identify transiently transfected cells for measurements of $[Ca^{2+}]_i$ in individual cells. HEK-Flp-In TREX-TRPV4 cells were generated and maintained as reported, and cells were incubated with tetracycline (100 ng/ml) for 16 h before study to induce TRPV4 expression (48). Cells were plated in poly-D-lysine-coated 96-well plates (BRET, Ca^{2+}, cAMP, ERK1/2 assays) or glass coverslips (microscopy, single cell Ca^{2+} assays) for 16–48 h before assays.

Cat-S Degradation of N-terminal PAR$_2$ Peptides—Peptides corresponding to N-terminal fragments of human PAR$_2$ (320–370 μM) were incubated with Cat-S (10 nM) in Hank's Balanced Salt Solution (HBSS) pH 7.4 for 0, 5, 30, or 60 min at 37 °C. Reactions were quenched with equal volume of 50% acetonitrile and 0.1% trifluoroacetic acid in H$_2$O. Degradation was assessed using an Agilent 1260 Infinity HPLC System with Poroshell 120, SB-C18, 2.1 × 30 mm, 2.7 μm column, 5–95% acetonitrile in water over 9 min, 0.1% TFA throughout. The reaction products were identified by mass spectrometry using a Shimadzu LCMS 2020, single quadrupole in electrospray in positive ionization mode with a mass range of 200–2000 m/z.

Cat-S Cleavage of Cell Surface PAR$_2$—HEK293 cells stably expressing human PAR$_2$ with N-terminal extracellular Flag and C-terminal intracellular HA11 epitopes were equilibrated in HBSS for 30 min, incubated with trypsin (100 nM), 2-furoyl-LIGRLO-NH$_2$ (10 μM), Cat-S (100 nM), Cat-S-AP (50 μM), or vehicle (control) for 30 min, and fixed with 4% paraformaldehyde (4 °C, 20 min). Cells were incubated in PBS containing 1% horse serum with mouse anti-Flag (2.5 μg/ml) and rat anti-HA (1:1000) antibodies (4 °C, overnight), washed and then incubated with Alexa-488 goat anti-mouse IgG and Alexa-597 goat anti-rat IgG secondary antibodies (1:1000, 1 h, room temperature). Images were obtained with Leica TCS SP8 Laser-scanning Confocal Microscope using a HCX PL APO ×63 oil immersion objective.

BRET Analysis of PAR$_2$ Association with Heterotrimeric G Proteins and β-Arrestins—PAR$_2$, G protein, and β-arrestin BRET was analyzed as described (48–50). For PAR$_2$ and G protein BRET, HEK-FT cells were transiently transfected with PAR$_2$-RLuc8 (0.18 μg), Gγ2-Venus (0.4 μg), Gβ1 (0.266 μg), and either Gαq or Gαs (0.266 μg) and using GeneJuice (Novagen). Gα was omitted from controls. For PAR$_2$ and β-arrestin BRET, HEK293 cells were transiently transfected with PAR$_2$-RLuc8 (1 μg) and β-arrestin1-YFP or β-arrestin2-YFP (4 μg). At 24 h after transfection, cells were seeded in 96-well plates. After 48 h, cells were equilibrated in HBSS for 30 min at 37 °C, and then incubated with the luciferase substrate coelenterazine H (Promega; 5 μM final) for 3 min. RLuc8 luminescence (480 nm) and Venus/YFP fluorescence (530 nm) were measured for a 2 min baseline and at various times after incubation with trypsin, Cat-S or Cat-S AP using LUMIstar Omega (BMG Labtech).

Signaling Assays in Cell Lines—For measurement of $[Ca^{2+}]_i$, cells were loaded with Fura-2/AM (1 μM) in assay buffer (150 mM NaCl, 2.6 mM KCl, 0.1 mM CaCl$_2$, 1.18 mM MgCl$_2$, 10 mM D-glucose, 10 mM HEPES, pH 7.4) containing 4 mM probenecid and 0.5% BSA for 1 h at 37 °C. For measurement of

$[Ca^{2+}]_i$ in cell populations, fluorescence was measured at 340 nm and 380 nm excitation and 530 nm emission using a FlexStation Microplate Reader (Molecular Devices). After a baseline reading for 60 s, cells were exposed to graded concentrations of trypsin or Cat-S, followed by ionomycin (10 μM) as a positive control. To examine Cat-S disarming of PAR$_2$, HEK293 cells were pre-incubated with vehicle (control) or Cat-S (100 nM) for 30 min, washed three times with assay buffer, and then challenged with trypsin (100 nM). For measurement of $[Ca^{2+}]_i$ in individual cells, cells were mounted in an open chamber and were observed using a Leica DMI6000B microscope with a HC PL APO 20× NA0.75 objective. Fluorescence was measured at 340 nm and 380 nm excitation with 530 nm emission using an Andor iXon 887 camera (Andor) and MetaFluor v7.8.0 software (Molecular Devices). Results are normalized to the ionomycin response or are expressed as change from basal in 340/380 nm ratio. cAMP accumulation was measured using the CAMYEL BRET sensor (48). HEK-PAR$_2$, KNRK-PAR$_2$, or KNRK-VC cells were transfected with 4 μg of cDNA encoding CAMYEL sensor (YFP-Epac-RLuc). In some experiments, KNRK cells were co-transfected with CAMYEL sensor plus 2 μg of wild-type PAR$_2$, a mutant of the Cat-S cleavage site (KNRK-PAR$_2\Delta$V^{55}S/E^{56}P/T^{57}K), or empty vector control pcDNA3.1. After 24 h, cells were seeded in 96-well plates and incubated overnight. Medium was replaced with HBSS 30 min before assays. Cells were loaded with coelenterazine H and BRET was measured as described above. After a 2-min basal period, cells were challenged with graded concentrations of trypsin, Cat-S, or Cat-S AP. Forskolin (10 μM) was used as a positive control. For assays of ERK activity, KNRK-PAR$_2$ cells were incubated in serum-free medium overnight. Cells were challenged at 37 °C with trypsin (100 nM) or Cat-S (100 nM) for 0–60 min for time course measurements, or with graded concentrations of trypsin or Cat-S for 5 min to generate concentration response curves. ERK1/2 activity was measured using AlphaScreen SureFire phosphor-ERK assay (PerkinElmer Life Sciences). FBS (10%) was used as a positive control.

Signaling Assays in Neurons—DRG (C1-L5) from C57BL/6 wild-type, *par2$^{-/-}$* or *trpv4$^{-/-}$* mice were dispersed by incubation in collagenase (2 mg/ml, Invitrogen) and dispase (2 mg/ml, Roche) for 30 min at 37 °C, triturated with a fire-polished Pasteur pipette, and incubated for an additional 20 min at 37 °C, triturated again, and incubated for an additional 10 min at 37 °C. Neurons were plated onto coverslips coated with laminin (0.004 mg/ml) and poly-D-lysine (0.1 mg/ml) in 12-well plates. Neurons were cultured in L-15 Lebovitz medium containing 10% fetal calf serum, with penicillin and streptomycin and maintained at 37 °C in a humidified atmosphere of 95% air and 5% CO$_2$ until retrieval (16 h) for signaling assays. For measurement of cAMP accumulation, neurons were preincubated with 3-isobutyl-1-methylxanthine (1 mM) for 45 min before assays. For assays of ERK activity, neurons were incubated in serum-free medium overnight. Neurons were challenged with trypsin (100 nM), Cat-S (100 nM), forskolin (10 μM, positive cAMP control), or phorbol 12,13-dibutyrate (200 nM, positive ERK1/2 control) for 30 min (cAMP assays) or 20 min (ERK1/2 assays) at 37 °C. cAMP accumulation was measured using AlphaScreen cAMP assay and ERK1/2 activity was measured using

AlphaScreen SureFire phosphor-ERK assay (PerkinElmer Life Sciences). For measurement of $[Ca^{2+}]_i$, neurons were loaded with Fura-2/AM (2 μM) and fluorescence was measured in individual neurons as described for cell lines. Neurons were challenged sequentially with either trypsin (100 nM) or Cat-S (100 nM), capsaicin (1 μM), and KCl (50 mM). In some experiments, neurons were assayed in Ca^{2+}-free buffer containing 2 mM EDTA. Neurons were also treated with inhibitors of PKA (PKI, 10 μM), adenylyl cyclase (SQ22536, 20 μM) or a TRPV4 antagonist (10 μM) (60-min preincubation). Images were analyzed using a custom journal in MetaMorph v7.8.2 software (Molecular Devices). A maximum intensity image was generated and projected through time to generate an image of all cells. Cells were segmented and binarized from this image using the Multi Wavelength Cell Scoring module on the basis of size and fluorescence intensity. Neurons of interest (< 25 μm diameter) were selected.

Cat-S Disarming of PAR₂ and Sensitization of TRPV4 in Xenopus Laevis Oocytes—Linearized plasmids were used as templates for cRNA synthesis (mMessage mMachine; Ambion) using T7 as promoter. Defolliculated stage V-VI oocytes were injected with cRNA encoding human PAR₂ alone (10 ng), human TRPV4 alone (0.5 ng) or both PAR2 (10 ng) plus TRPV4 (0.5 ng). The cRNAs were dissolved in RNase-free water and the total volume injected was 46 nl. Injected oocytes were stored at 19 °C in ND96 solution (in mM: NaCl 96, KCl 2, CaCl₂ 1.8, MgCl₂ 1, HEPES 5, pH 7.4 with Tris) supplemented with 100 units/ml penicillin and 100 μg/ml streptomycin. Oocytes were studied 2 days after injection using the two-electrode voltage-clamp technique in nominally free Ca^{2+} solution (45). Individual oocytes were superfused (2–3 ml/min) with Ca^{2+}-free solution (in mM: NaCl 96, KCl 2, MgCl₂ 1, HEPES 5, EGTA 1, pH 7.4 with NaOH) at room temperature. To examine disarming of PAR₂, oocytes expressing PAR₂ alone were pre-incubated with Cat-S (1 μM), Cat-S AP (50 μM), trypsin (8 nM), or vehicle (control) for 5 min, and whole-cell currents were measured after challenge with trypsin (8 nM). To examine PAR₂-dependent sensitization of TRPV4, oocytes expressing TRPV4 alone or TRPV4 plus PAR₂ were pre-incubated with trypsin (8 nM), Cat-S (1 μM) or Cat-S AP (50 μM) for 5 min, and whole-cell currents were measured after challenge with GSK1016790A (50 nM) and HC067047 (100 nM). All recordings were obtained at a holding potential of -60 mV. Downward deflections in the current traces correspond to inward currents (*i.e.* movement of positive charge into the cell). Recordings were obtained using an OC-725C amplifier (Warner Instruments Corp.) and were analyzed using PULSE 8.67 software (HEKA).

Cat-S Sensitization of TRPV4 in HEK Cells—$[Ca^{2+}]_i$ was measured in individual HEK-TRPV4 cells as described above. Cells were pre-incubated with Cat-S (100 nM), trypsin (100 nM), or vehicle for 5 min, and then challenged with GSK1016790A (100 pM). The maximal increase in $[Ca^{2+}]_i$ above basal within 15 min of challenge with GSK1016990A was determined.

Cat-S hyperexcitability of Nociceptive Neurons—DRG (T9-T13) from C57BL/6 mice were dispersed by incubation in collagenase (1 mg/ml, Worthington) and dispase (4 mg/ml, Roche) for 10 min at 37 °C, triturated with a fire-polished Pasteur pipette, and incubated for an additional 5 min at 37 °C. Neurons

were plated onto coverslips coated with laminin (0.017 mg/ml) and poly-D-lysine (2 mg/ml) in 24-well plates. Neurons were cultured in F12 medium containing 10% fetal calf serum, with penicillin and streptomycin and maintained at 37 °C in a humidified atmosphere of 95% air and 5% CO_2 until retrieval (16 h) for electrophysiological studies. Cells were pre-incubated with Cat-S (500 nM) for 1 h. The PKA inhibitors PKI (10 μM) or H-89 (10 μM), the adenylyl cyclase inhibitor SQ22536 (20 μM) or the PKC inhibitor GF-109203X (10 μM) were applied 30 min before Cat-S. Perforated patch-clamp recordings were made using amphotericin B (240 g/ml, Sigma Aldrich) from small-diameter neurons (<30 pF capacitance) in current clamp mode at room temperature. Changes in excitability were quantified by measuring rheobase and numbers of action potentials discharged at twice rheobase. Recordings were made using Multiclamp 700B or Axopatch 200B amplifiers, digitized by Digidata 1440A or 1322A and stored and processed using pClamp 10.1 software (Molecular Devices). The recording chamber was continuously perfused with external solution at 2 ml/min. Solutions has the following composition (mM): pipette solution: K-gluconate 110, KCl 30, HEPES 10, MgCl₂ 1, CaCl₂ 2; pH 7.25 with 1 M KOH; external solution - NaCl 140, KCl 5 HEPES 10, glucose 10, MgCl₂ 1, CaCl₂ 2; pH to 7.3 to 7.4 with 3 M NaOH.

Mechanical Hyperalgesia and Edema in Mice—For behavioral assessments, mice were placed in individual cylinders on a mesh stand. Mice were acclimatized to the experimental room, restraint apparatus, and investigator for 2-h periods on 2 successive days before experiments, and the investigator was blinded to the experimental treatments. To assess mechanical pain, paw withdrawal in response to stimulation of the plantar surface of the hind paw with graded von Frey filaments (0.078, 0.196, 0.392, 0.686, 1.569, 3.922, 5.882, 9.804, 13.725, and 19.608 mN) was determined using the "up-and-down" paradigm (51). In this analysis, an increase in the filament stiffness required to induce paw withdrawal indicates mechanical analgesia, whereas a decrease in the filament stiffness required to induce withdrawal indicates mechanical hyperalgesia. To assess inflammatory edema of the paw, hind paw thickness was measured using digital calipers before and after treatments (52). On the day before the study, von Frey scores were measured in triplicate to establish a baseline for each animal. To examine the effects of Cat-S, mice were sedated with 5% isoflurane and Cat-S (1.4–14 μM, 10 μl) or vehicle (0.9% NaCl, 10 μl) was injected subcutaneously into the plantar surface of one hind paw. To evaluate the contribution of cAMP to Cat-S evoked pain, the adenylyl cyclase inhibitor SQ22536 (1 μg in 2.5 μM in 10 μl) or vehicle (0.9% NaCl) was injected into the paw 30 min before Cat-S (2.5 μM, 10 μl). Injection of SQ22563 or vehicle was preceded by an injection of 2.5 μl distilled water to cause a transient hyposmotic permeabilization. To investigate the contribution of Cat-S and PAR₂ in formalin-induced pain and inflammation, mice were pre-treated with Cat-S inhibitor MV026031 (50 mg/kg), PAR₂ antagonist GB88 (10 mg/kg) or vehicle by gavage. Formalin (4%, 10 μl) or NaCl (0.9%, 10 μl) was injected into the plantar surface of the hindpaw 2 h later. Mechanical hyperalgesia and edema were measured between 30–240 min after intraplantar injections. Afterward, the paws were collected for Cat-S activity assays.

Cat-S Activity Assays—Paws were removed 4 h after formalin or saline injection. The skin of the pad was excised, homogenized, and sonicated in HBSS, and centrifuged (20,000 × g, 15 min, 4 °C). Supernatants (10 μg protein) were incubated with 50 μM Cat-S substrate Acetyl-KQKLR-AMC in the presence or absence of Cat-S inhibitor MV026031 (1 μM) for 30 min at 37 °C. Fluorescence was measured at 354 nm excitation and 442 nm emission. Activity that was susceptible to inhibition by MV026031 was attributed to Cat-S and results are expressed as fold-change over saline-treated tissues.

Statistical Analyses—Results are expressed as mean ± S.E. Differences between two groups were examined using unpaired *t*-tests. Differences between multiple groups were examined using an ANOVA and a Bonferroni's or Dunnett's post-hoc test. A *p* value <0.05 was considered to be significant.

RESULTS

Cat-S Cleaves within the Extracellular N Terminus of Human PAR$_2$ at $E^{56} \downarrow T^{57}$—To determine whether Cat-S can cleave PAR$_2$, we incubated recombinant human Cat-S (10 nM) with three 30 residue peptides (320–370 μM) corresponding to most of the amino terminus of PAR$_2$ (residues 21–90) and examined degradation by high pressure liquid chromatography (HPLC) and mass spectrometry (Fig. 1A). Cat-S rapidly degraded the PAR$_2$ 31–60 fragment, with detectable degradation after 5 min and ~50% degradation after 60 min (Fig. 1B). Two products were identified, corresponding to PAR$_2$ 31–56 and PAR$_2$ 57–60. These findings indicate that Cat-S hydrolyzes PAR$_2$ 31–60 at $E^{56} \downarrow T^{57}$, 20 residues downstream of the canonical trypsin cleavage site $R^{36} \downarrow S^{37}$. Cat-S did not degrade PAR$_2$ 21–50 after 60 min (Fig. 1C), and there was minimal degradation of PAR$_2$ 61–90 after 60 min (Fig. 1D). Thus, Cat-S cleaves at a major single site within the extracellular N terminus of human PAR$_2$: $E^{56} \downarrow T^{57}$.

Cat-S Cleaves PAR$_2$ Expressed in HEK Cells but Does Not Stimulate Receptor Endocytosis—Although Cat-S can hydrolyze a synthetic fragment of PAR$_2$, steric restrictions or the presence of other components in the plasma membrane could affect cleavage of the intact receptor in cells. To assess whether Cat-S can cleave the PAR$_2$ at the plasma membrane, we expressed in HEK293 cells human PAR$_2$ with an extracellular N-terminal Flag epitope and an intracellular C-terminal HA11 epitope (Fig. 2A). We exposed the cells to vehicle, proteases or synthetic PAR$_2$ agonists, and localized Flag and HA11 epitopes by immunofluorescence and confocal microscopy. In cells treated with vehicle, Flag and HA11 remained at the plasma membrane (Fig. 2B). After incubation with trypsin (100 nM, 30 min), Flag was removed from the cell surface and HA11 was detected in endosomes (Fig. 2C). This result is consistent with trypsin cleavage of PAR$_2$, which would remove the Flag epitope, expose the canonical tethered ligand, and activate and internalize the cleaved receptor, as we have previously described (46, 47). After incubation with 2-furoyl-LIGRLO-NH$_2$ (10 μM, 30 min), a synthetic analog of the trypsin-revealed tethered ligand and a potent PAR$_2$ agonist (53), both Flag and HA11 were colocalized in endosomes, consistent with receptor activation and endocytosis without cleavage (Fig. 2C). After incubation with Cat-S (100 nM, 30 min), Flag was removed yet HA11

remained at the cell surface (Fig. 2D). Cat-S cleavage of PAR$_2$ at $E^{56} \downarrow T^{57}$ would expose a potential tethered ligand domain beginning ^{57}TVFSV. Incubation of cells with the decapeptide TVFSVDEFSA (50 μM, 30 min), which corresponds to the putative tethered ligand and is hereafter referred to as Cat-S activating peptide (AP), did not affect the subcellular localization of Flag or HA11, which remained at the plasma membrane (Fig. 2D). Thus, trypsin cleaves and activates PAR$_2$, which results in receptor endocytosis. Although Cat-S cleaves PAR$_2$, it does not trigger receptor endocytosis. Whereas the trypsin-revealed AP stimulates PAR$_2$ endocytosis, Cat-S AP is unable to internalize this receptor.

Cat-S Removes the Canonical Trypsin Cleavage Site and the Trypsin-exposed Tethered Ligand and Prevents Trypsin-induced Activation of PAR$_2$—Cat-S cleavage of PAR$_2$ at $E^{56} \downarrow T^{57}$ would be expected to remove the trypsin-exposed tethered ligand domain (^{37}SLIGKV^{42}), which is upstream of the Cat-S site, and thereby prevent trypsin-induced activation of this receptor, as we have previously reported for elastase (33, 46). To examine this possibility, we pre-incubated HEK293 cells, which express endogenous PAR$_2$, with vehicle (control) or Cat-S (100 nM) for 30 min. Cells were washed and trypsin (100 nM)-evoked increases in $[Ca^{2+}]_i$ were measured to assess PAR$_2$ activation (Fig. 3A). In cells treated with vehicle, trypsin caused a rapid and transient increase in $[Ca^{2+}]_i$ (Fig. 3B). Pre-incubation with Cat-S caused a >2-fold reduction in the response to trypsin (Fig. 3, B and C). Since HEK cells also express PAR$_1$, which can also be activated by trypsin (15), we confirmed the specific attenuation of PAR$_2$ activation in *Xenopus laevis* oocytes. We expressed PAR$_2$ in oocytes and examined trypsin-evoked PAR$_2$ activation by measurement of whole-cell currents using the two-electrode voltage-clamp technique. In oocytes pre-incubated with vehicle, trypsin (8 nM) stimulated a transient inward current, consistent with the activation of Ca^{2+}-sensitive Cl^- channels (Fig. 3, D–F). There was no or minimal response to trypsin in non-injected oocytes, which indicates the requirement of PAR$_2$ expression for the trypsin response (not shown). Pre-incubation with trypsin (8 nM, 5 min), abolished the response to subsequent trypsin challenge (Fig. 3, E and F), consistent with PAR$_2$ cleavage, exposure of the tethered ligand, and desensitization (54). Pre-incubation with Cat-S (1 μM, 5 min) suppressed trypsin-evoked currents by >3-fold (Fig. 3, E and F). Our results suggest that Cat-S removes the canonical trypsin cleavage site and trypsin-exposed tethered ligand and thereby disarms PAR$_2$. Notably, pre-incubation of oocytes with Cat-S AP (50 μM, 5 min) also inhibited trypsin-evoked currents by >2-fold (Fig. 3, E and F). A possible explanation for this effect is that Cat-S AP can activate PAR$_2$ and thereby desensitize responses to trypsin PAR$_2$, as is the case for the trypsin-exposed AP, which desensitizes PAR$_2$ (54).

Cat-S Stimulates PAR$_2$ Coupling to Gαs but Not Gαq—After interaction with agonists, GPCRs adopt conformational changes that facilitate coupling to heterotrimeric G-proteins, which initiate intracellular signaling events. Trypsin cleavage of PAR$_2$ leads to mobilization of intracellular Ca^{2+}, which is consistent with PAR$_2$ coupling to Gαq, activation of phospholipase Cβ and formation of inositol trisphosphate. To determine whether Cat-S also induces coupling of PAR$_2$ to heterotrimeric
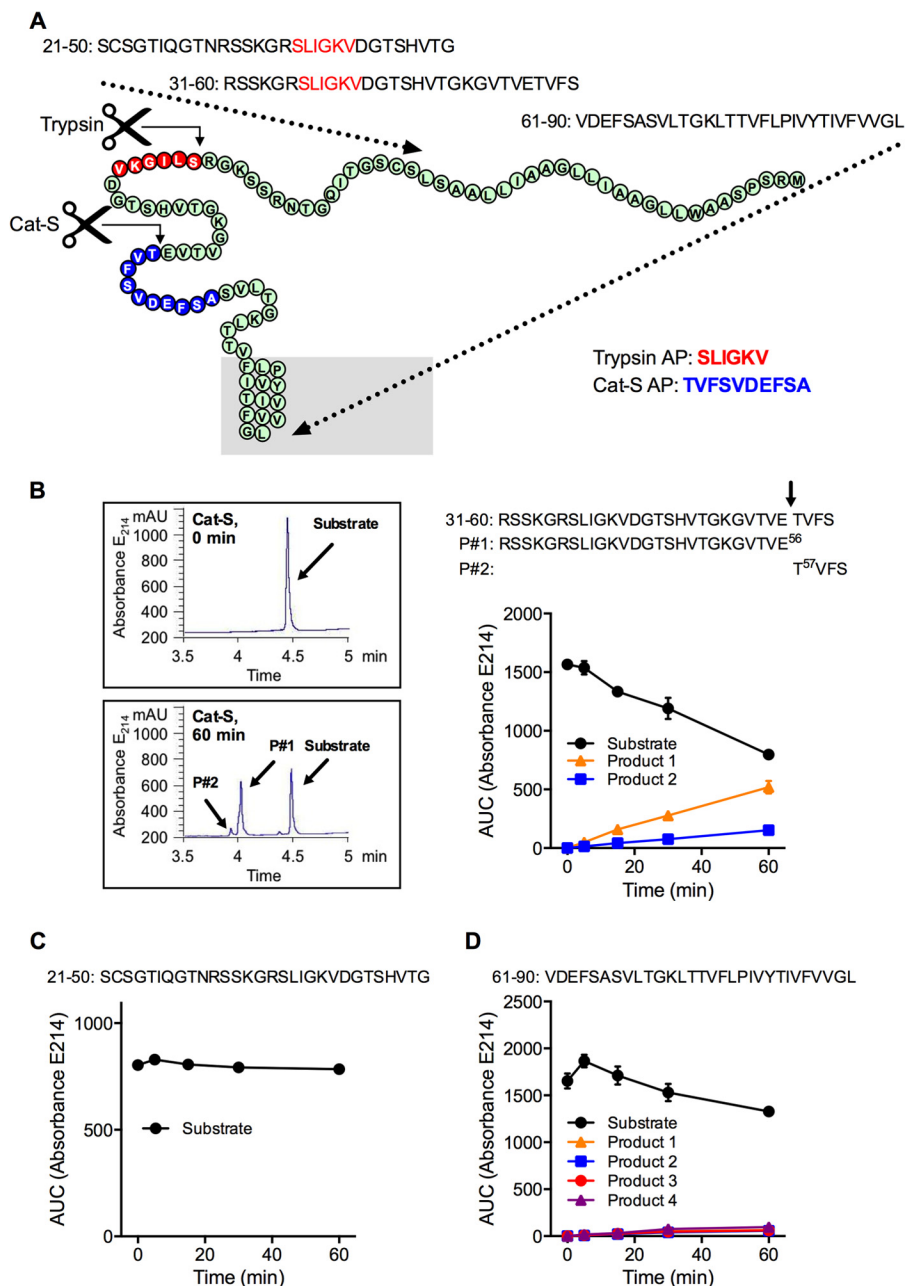
FIGURE 1. **Cat-S degradation of N-terminal fragments of human PAR_2.** *A*, N terminus of human PAR_2 showing the sequences of the synthetic peptides that were used for degradation studies. The residues in *red* denote the canonical tethered ligand and a corresponding AP that is revealed after trypsin cleavage. The residues in *blue* denote the presumed tethered ligand and a corresponding AP that would be revealed after Cat-S cleavage. *Gray shading* represents membrane. *B*, Cat-S degradation of PAR_2 31–60. HPLC traces (*left*) show elution of the substrate and products (*P*) after incubation with Cat-S for 0 min or 60 min. Time course (*right*) shows the kinetics of substrate degradation and product formation. Analysis of the products is consistent with Cat-S cleaving human PAR_2 at $E^{56} \downarrow T^{57}$. *C*, time course of levels of PAR_2 21–50 after incubation with Cat-S, showing no detectable degradation. *D*, time course of levels of PAR_2 61–90 after incubation with Cat-S, showing minimal degradation and the appearance of 4 minor products that were not identified. $n = 3$ experiments.

G proteins, we used bioluminescence resonance energy transfer (BRET) to examine changes in conformation/proximity between PAR_2 and Gγ in response to different ligands (Fig. 4A). We expressed in HEK293 cells PAR_2 with a C-terminal RLuc8 together with Gγ2-Venus, Gβ1 and various Gα subunits. By expressing either Gαq or Gαs, we were able to assess PAR_2 coupling to different Gα subunits, as described for other GPCRs (49). Thus, a change in the agonist-induced BRET signals (increase or decrease) in cells overexpressing Gα subunits would suggest a conformational change in the receptor that favors coupling to the Gα subunits in question. Cells not transfected with Gα were used as a control. In control cells, trypsin (100 nM), Cat-S (100 nM), or Cat-S AP (10 μM) did not affect the BRET signal between PAR_2-RLuc8 and Gγ2-Venus (Fig. 4B). In cells overexpressing Gαq, trypsin caused a rapid increase in BRET that was maximal at 6 min, sustained for 8 min, and declined to baseline after 10 min (Fig. 4C). This finding suggests that trypsin induces a conformational change in PAR_2 that facilitates coupling to Gαq, which would lead to the expected mobilization of intracellular Ca^{2+} stores. In contrast, Cat-S did
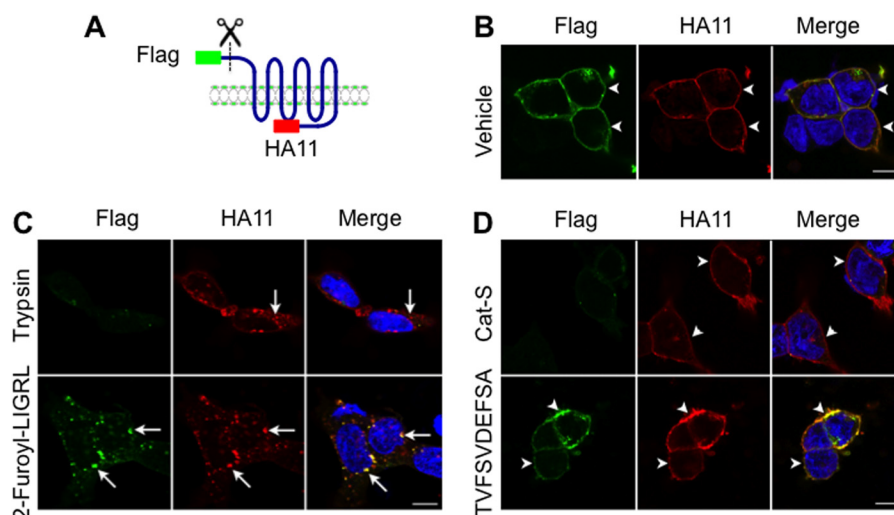
FIGURE 2. **Cat-S removal of extracellular epitope of human PAR$_2$.** *A*, human PAR$_2$ with N-terminal Flag and C-terminal HA11 epitopes that was expressed in HEK cells. *B–D*, confocal photomicrographs showing immunoreactive Flag (*green*) and HA11 (*red*) epitopes after incubation with vehicle (*B*), trypsin (100 nM) or 2-furoly-LIGRLO-NH$_2$ (10 μM) (*C*), or Cat-S (100 nM) or TVFSVDEFSA (50 μM) (*D*). *Arrowheads* show plasma membrane and arrows show endosomes. Scale bar, 10 μm. Representative images from three experiments.
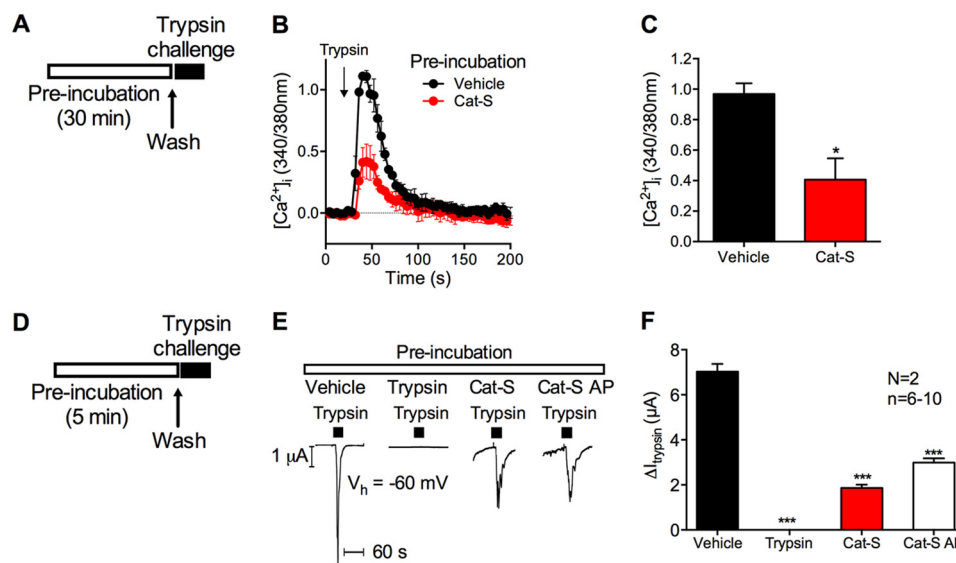
FIGURE 3. **Cat-S removal of the canonical tethered ligand and inhibition of trypsin-evoked activation of PAR$_2$.** *A*, HEK293 cells were pre-incubated with vehicle (control) or Cat-S (100 nM) for 30 min, washed and then challenged with trypsin (*arrow*, 100 nM). Changes in $[Ca^{2+}]_i$ were measured using Fura-2/AM. *B*, trypsin responses in cells pre-incubated with vehicle or Cat-S (*n* = 3). *C*, maximal trypsin responses in cells pre-incubated with vehicle or Cat-S (*n* = 3). *, $p < 0.05$ compared with vehicle. *D*, *Xenopus laevis* oocytes expressing PAR$_2$ were pre-incubated with vehicle (control), trypsin (8 nM), Cat-S (1 μM), or Cat-S AP (50 μM) for 5 min. After pre-incubation, trypsin (8 nM)-evoked whole-cell currents (*black bar*) were measured. *E*, representative whole-cell current traces. *F*, mean $\Delta I_{trypsin}$ values of pooled experiments. *n* indicates number of individual oocytes studied. *N* indicates the number of batches of oocytes. ***, $p < 0.001$ compared with vehicle.

not induce BRET in cells overexpressing Gαq. In cells overexpressing Gαs, both Cat-S and trypsin caused a change in BRET that was maximal after 5 min, but in opposite directions, and BRET returned to baseline after 10 min (Fig. 4*D*). These results suggest that Cat-S- and trypsin-activated PAR$_2$ couples to Gαs, which would be expected to activate adenylyl cyclase and generate cAMP. The opposite direction of BRET signal suggests that Cat-S and trypsin induce distinct conformational changes in PAR$_2$. Cat-S AP also caused a large change in BRET in Gαs-transfected cells, but here the BRET signal rapidly declined (Fig. 4*E*). Considered together, our results suggest that trypsin, Cat-S and Cat-S AP can all affect BRET signal between PAR$_2$-RLuc8 and Gγ2-Venus, but that the magnitude and direction of the

change depends on the agonist and on the overexpressed Gα subunits. It is probable that different proteases and peptide agonists stabilize distinct conformations of PAR$_2$ that favor coupling to particular heterotrimeric G proteins. These differences are not attributable to altered levels of Gγ2-Venus expression, which were similar in all experiments (Fig. 4*F*). Thus, Cat-S causes PAR$_2$ coupling to Gαs but not Gαq, which would lead to formation of cAMP but not mobilization of intracellular Ca^{2+} stores.

Cat-S Stimulates PAR$_2$-dependent Formation of cAMP but Not Ca^{2+} Mobilization, ERK1/2 Activation, or β-Arrestin Recruitment—After activation with trypsin, PAR$_2$ couples to Gαq and mobilization of intracellular Ca^{2+}, to Gαs and gener-
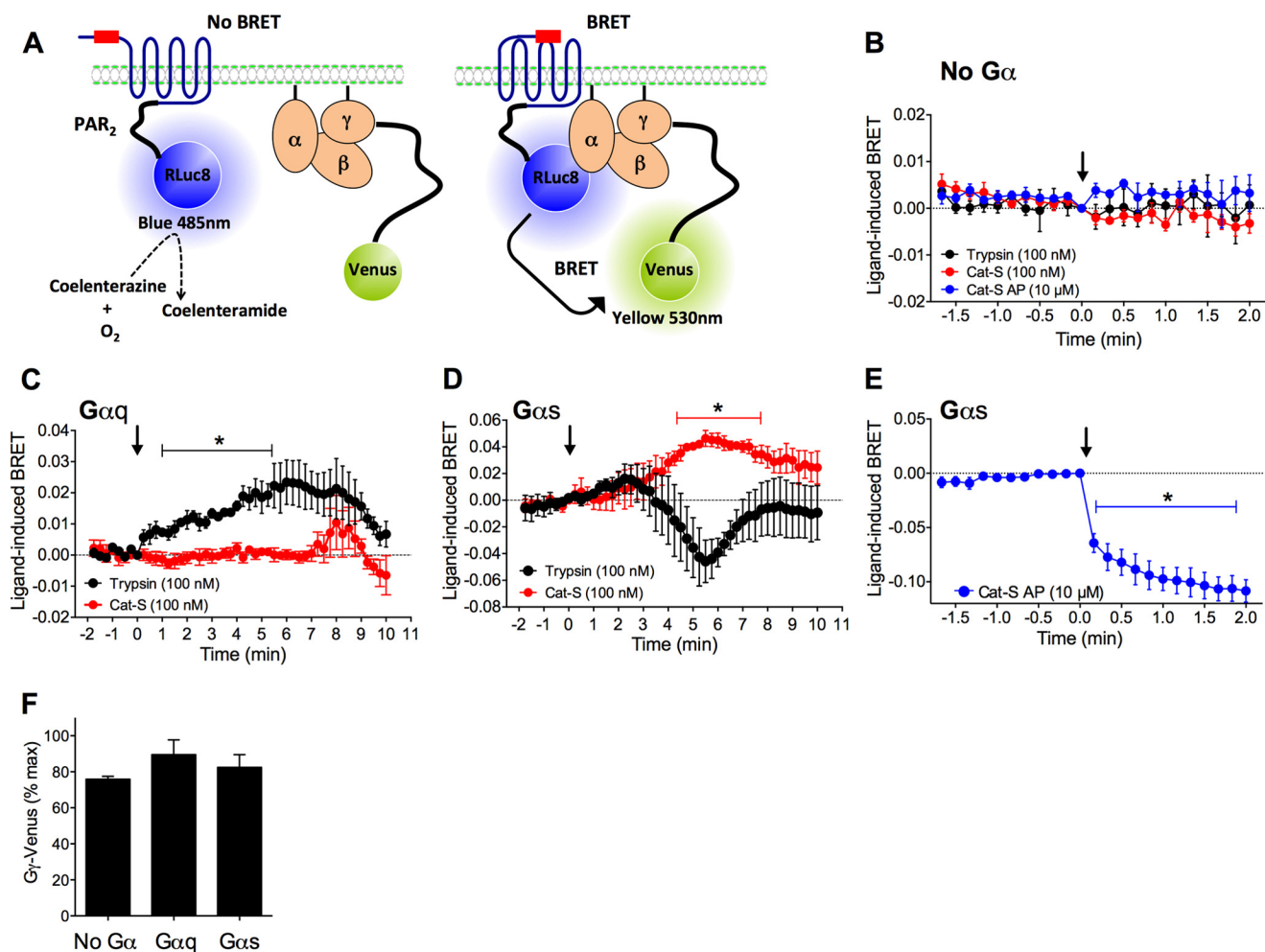
FIGURE 4. **PAR₂ and G-protein interactions by BRET.** *A*, PAR₂-RLuc8 and GγVenus were co-expressed in HEK293 cells with Gβ1 and various Gα subunits. Upon activation, alterations in the conformation PAR₂-RLuc8 and its proximity to GγVenus generates a change in the BRET signal. *B–E*, effects of trypsin (100 nM), Cat-S (100 nM), or Cat-S AP (10 μM) (*arrows*) on BRET in cells not overexpressing Gα (*B*), in cells overexpressing Gαq (*C*), and in cells overexpressing Gαs (*D, E*). *F* shows the GγVenus fluorescence. Duplicate measurements of $n = 3–4$ experiments. *, $p < 0.05$ compared with basal.

ation of cAMP, and to β-arrestins which mediate receptor endocytosis and activation of extracellular signal regulated kinases 1/2 (ERK1/2) from endosomal signalosomes (11). To examine PAR₂-dependent signals, we compared responses of KNRK cells expressing human PAR₂ (KNRK-PAR₂) or empty vector control (KNRK-VC). We also examined signaling in HEK293 cells overexpressing PAR₂, and used the Cat-S inhibitor MV026031 and the PAR₂ antagonist GB88 (55) to ascertain the respective requirements of enzymatic activity and PAR₂ activation for responses.

As we have previously shown, trypsin stimulated a rapid, transient and concentration-dependent increase in $[Ca^{2+}]_i$ in KNRK-PAR₂ cells but not in KNRK-VC cells (12) (Fig. 5). Cat-S did not affect $[Ca^{2+}]_i$ in KNRK-PAR₂ cells at any concentration or time point studied (Fig. 5).

We first studied cAMP signaling in HEK-PAR₂ cells, which were readily transfected with PAR₂ and the CAMYEL YFP-Epac-RFP cAMP sensor. Trypsin stimulated a rapid, transient and concentration-dependent increase in cAMP formation in HEK-PAR₂ cells (Fig. 6, *A* and *B*). Cat-S also caused a time and concentration-dependent increase in cAMP formation in HEK-PAR₂ cells, with an EC_{50} of 128 ± 4.0 nM, similar to that of

trypsin (Fig. 6, *A* and *B*). The effect of Cat-S (100 nM) was abolished when the protease was pre-incubated with the selective Cat-S inhibitor MV026031 (1 μM, 30 min before assay), and is thus dependent on enzymatic activity (Fig. 6C). Pre-incubation of HEK-PAR₂ cells with the PAR₂ antagonist GB88 (10 μM, 60 min) (55) abolished the cAMP response to Cat-S (Fig. 6C). Cat-S (100 nM) also stimulated cAMP generation in KNRK-PAR₂ cells, and had a small stimulatory effect in KNRK-VC cells, presumably by a PAR₂-independent process since KNRK-VC cells do not express appreciable levels of PAR₂ (Fig. 6D). Cat-S AP caused a concentration-dependent stimulation of cAMP formation in KNRK-PAR₂ cells but not in KNRK-VC cells (EC_{50} 6.85 ± 0.33 μM, Fig. 6E). A control peptide in which the first 2 residues were substituted (PGFSVDEFSA) had no effect on cAMP formation in KNRK-PAR₂ or KNRK-VC cells (Fig. 6F).

Trypsin-activated PAR₂ interacts with β-arrestins, which mediate endocytosis of PAR₂ and assemble signalosomes that are required for ERK1/2 activation (36, 47). To determine whether Cat-S induces interaction between PAR₂ and β-arrestins, we coexpressed PAR₂-RLuc8 and β-arrestin1-YFP or β-arrestin2-YFP in HEK293 cells, and examined protease-in-
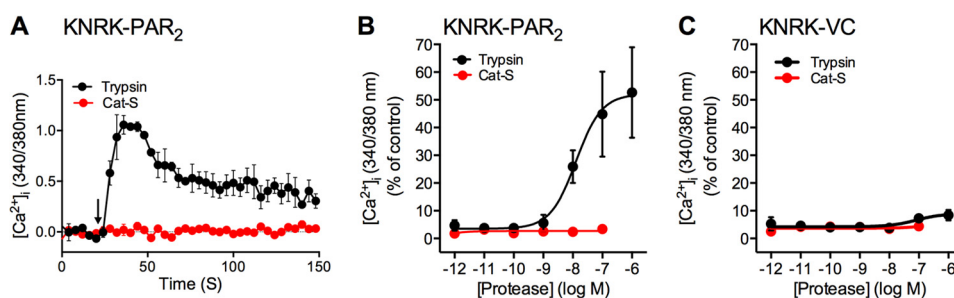
FIGURE 5. **PAR₂-dependent mobilization of intracellular Ca²⁺.** $[Ca^{2+}]_i$ was measured in KNRK-PAR₂ or KNRK-VC cells. *A*, time course of effects of trypsin (100 nM) and Cat-S (100 nM) (*arrows*) on $[Ca^{2+}]_i$ in KNRK-PAR₂ cells. *B* and *C*, effect of graded concentrations of trypsin and Cat-S on $[Ca^{2+}]_i$ in KNRK-PAR₂ cells (*B*) and KNRK-VC cells (*C*). Results are normalized to the ionomycin (positive control) response. Triplicate measurements of *n* = 3–4 experiments.
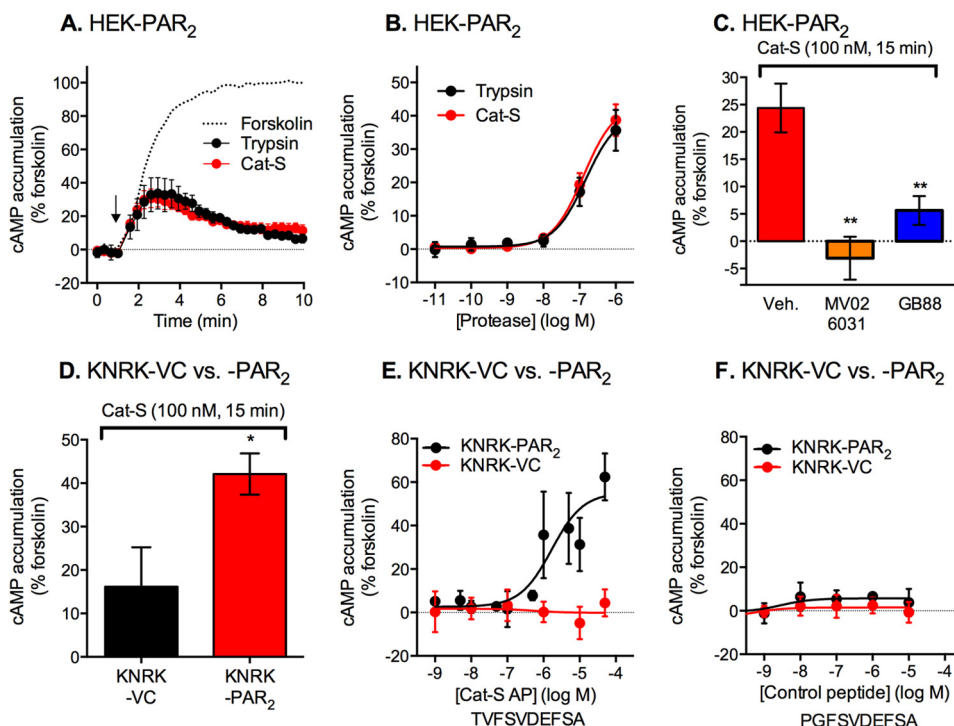
FIGURE 6. **PAR₂-dependent formation of cAMP.** cAMP formation was measured in HEK-PAR₂ cells (*A–C*) or in KNRK-PAR₂ or KNRK-VC cells (*D–F*). *A*, effects of trypsin (100 nM), Cat-S (100 nM), and forskolin (10 μM) (*arrow*) on cAMP formation. *B*, effects of graded concentrations of trypsin and Cat-S on cAMP formation. *C*, effects of Cat-S (100 nM) on cAMP formation in HEK-PAR₂ cells. Cat-S was pretreated with the inhibitor MV026031 or cells were preincubated with the PAR₂ antagonist GB88. *D*, effects of Cat-S (100 nM) on cAMP formation in KNRK-PAR₂ and KNRK-VC cells. *E* and *F*, effects of Cat-S AP (TVFSVDEFSA) (*E*) and control peptide (PGFSVDEFSA) (*F*) on cAMP formation in KNRK-PAR₂ or KNRK-VC cells. Triplicate measurements of *n* = 3–4 experiments. *, $p < 0.05$; **, $p < 0.01$ compared with vehicle (*veh.*) or KNRK-VC cells.

duced BRET signals (50). As we have previously reported, trypsin stimulated a time- and concentration-dependent BRET between PAR₂-RLuc8 and β-arrestin1-YFP or β-arrestin2-YFP (48) (Fig. 7, *A–D*). Cat-S did not induce a detectable BRET signal at any time or concentration tested (Fig. 7, *A–D*). The inability of Cat-S to recruit β-arrestins is in accordance with the finding that Cat-S did not stimulate endocytosis of PAR₂ (Fig. 2*A*), and agrees with our report that β-arrestins mediate endocytosis of trypsin-activated PAR₂ (47). Challenge of KNRK-PAR₂ cells with trypsin stimulated a rapid and concentration-dependent activation of ERK1/2, whereas Cat-S did not stimulate ERK1/2 activation (Fig. 7, *E* and *F*). These findings are consistent with the report that β-arrestins mediate PAR₂-mediated ERK1/2 activation in KNRK-PAR₂ cells (36).

Our results suggest that Cat-S is a biased agonist of PAR₂. In contrast to trypsin, which mobilizes intracellular Ca²⁺, generates cAMP and recruits β-arrestins that mediate PAR₂ endocy-

tosis and ERK1/2 activation, Cat-S stimulates only PAR₂-dependent formation of cAMP. The observation that Cat-S AP also stimulates PAR₂-dependent cAMP formation suggests that the stimulatory action of Cat-S, like that of trypsin, involves proteolytic exposure of a tethered ligand.

Cat-S-evoked Activation of PAR₂ Requires Receptor Cleavage—To verify the requirement of PAR₂ cleavage for Cat-S signaling, we mutated the putative cleavage site. We first determined whether Cat-S cleaved a decapeptide in which the P2, P1, and P1′ positions were substituted: $V^{55} \rightarrow S$, $E^{56} \rightarrow P$, and $T^{57} \rightarrow K$ (^{52}GVTSPKVFSVD^{62}). As expected, Cat-S was unable to cleave this peptide at concentration up to 880 μM (Fig. 8*A*). Thus, when Cat-S (10 nM) was incubated with G^{52}VTSPKVFSVD^{62} for 60 min, 6.6 ± 1.4% of the fragment was degraded. In comparison, when Cat-S was incubated with PAR₂ 31–60 under the same conditions for 60 min, 49.1 ± 0.2% of the fragment was degraded (Fig. 1*B*). We then mutated the equiv-
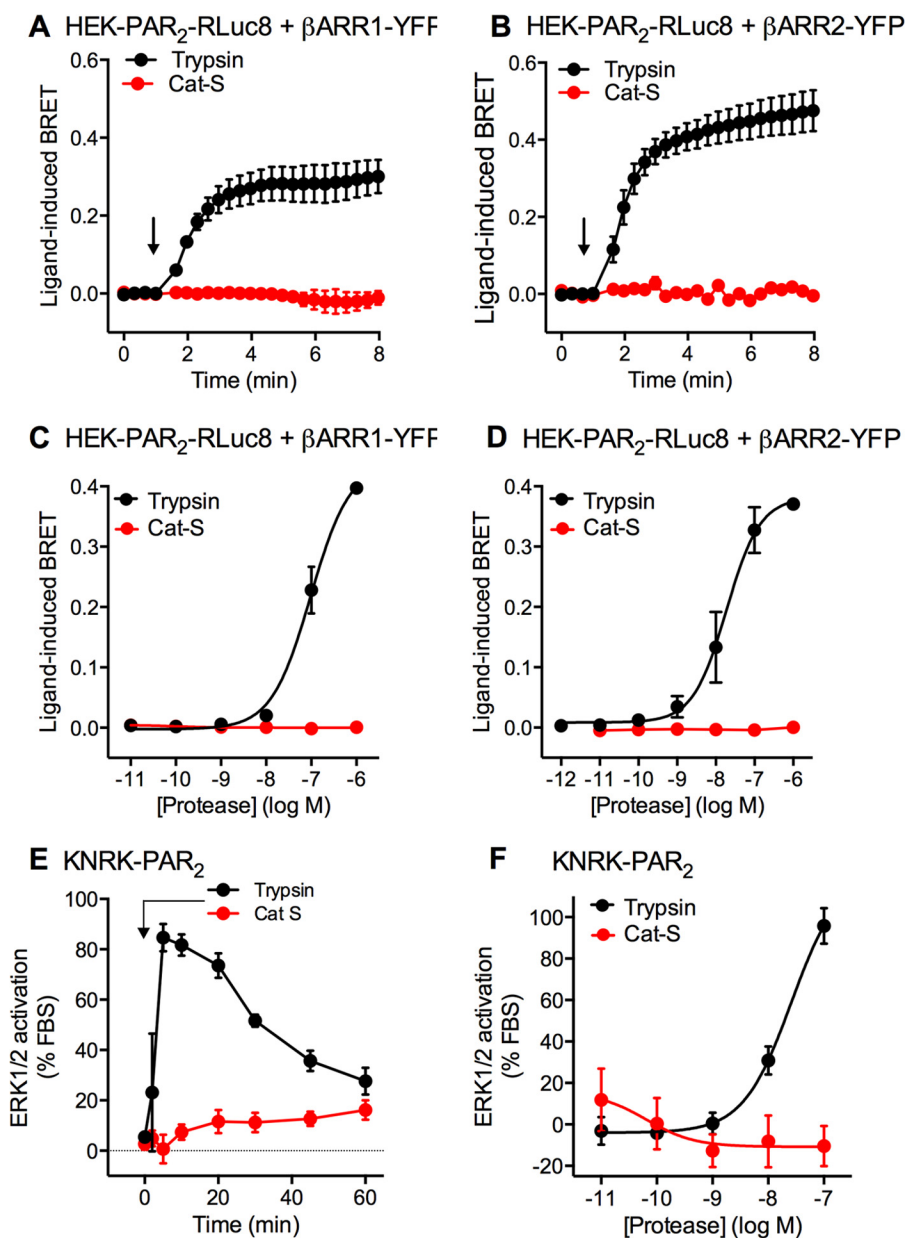
FIGURE 7. **PAR$_2$-dependent recruitment of β-arrestins by BRET and activation of ERK1/2.** *A–D*, PAR$_2$-RLuc8 and β-arrestin1-YFP (*A*, *C*) or β-arrestin2-YFP (*B*, *D*) were coexpressed in HEK293 cells, and ligand-induced BRET was examined. *A* and *B*, time course of effects trypsin (100 nM) and Cat-S (100 nM) (*arrows*). *C* and *D*, effects of graded concentrations of trypsin and Cat-S. *E* and *F*, time course of effects of trypsin (100 nM) and Cat-S (100 nM) (*E*) and concentration-response analysis (*F*) on ERK1/2 activation in KNRK-PAR$_2$ cells. Triplicate measurements of $n = 3–4$ experiments.

alent residues in human PAR$_2$ and transiently expressed the mutant (PAR$_2\Delta$V^{55}S/E^{56}P/T^{57}K) or wild-type PAR$_2$ (both with C-terminal HA11 epitopes) in HEK293 or KNRK cells. PAR$_2\Delta$V^{55}S/E^{56}P/T^{57}K, like PAR$_2$ wild-type, was normally localized at the plasma membrane of HEK cells (Fig. 8*B*). Trypsin similarly increased [Ca^{2+}]$_i$ in KNRK-PAR$_2\Delta$V^{55}S/E^{56}P/ T^{57}K and in KNRK-PAR$_2$ cells (Fig. 8*C*). However, whereas Cat-S stimulated a concentration-dependent formation of cAMP in KNRK-PAR$_2$ cells, Cat-S did not stimulate cAMP formation in KNRK-PAR$_2\Delta$V^{55}S/E^{56}P/T^{57}K cells (Fig. 8*D*). Our results suggest that Cat-S cleaves PAR$_2$, which activates adenylyl cyclase and generates cAMP.

Cat-S Induces PAR$_2$-dependent Sensitization of TRPV4— Trypsin-cleaved PAR$_2$ can activate and sensitize TRPV4 by mechanisms that involve channel phosphorylation by protein

kinase C (PKC) and tyrosine kinases, and the generation of arachidonic acid metabolites that directly activate TRPV4, which result in inflammation and hyperalgesia (28–30). To determine whether Cat-S-activated PAR$_2$ can sensitize TRPV4, we expressed in *Xenopus laevis* oocytes human TRPV4 alone or TRPV4 plus human PAR$_2$. We exposed oocytes to vehicle (control), trypsin (8 nM), Cat-S (1 μM) or Cat-S AP (50 μM) for 5 min, and then activated TRPV4 with the selective agonist GSK1016790A (50 nM) followed by the TRPV4 antagonist HC067047 (100 nM). We compared the magnitude of the response to the TRPV4 agonist in oocytes expressing TRPV4 alone to that in oocytes expressing PAR$_2$ plus TRPV4. In vehicle-treated oocytes expressing TRPV4 alone, GSK1016790A caused a small inward current that was reversed by HC067047 and is thus attributable to TRPV4 activation (Fig. 9*A*). Pretreat-
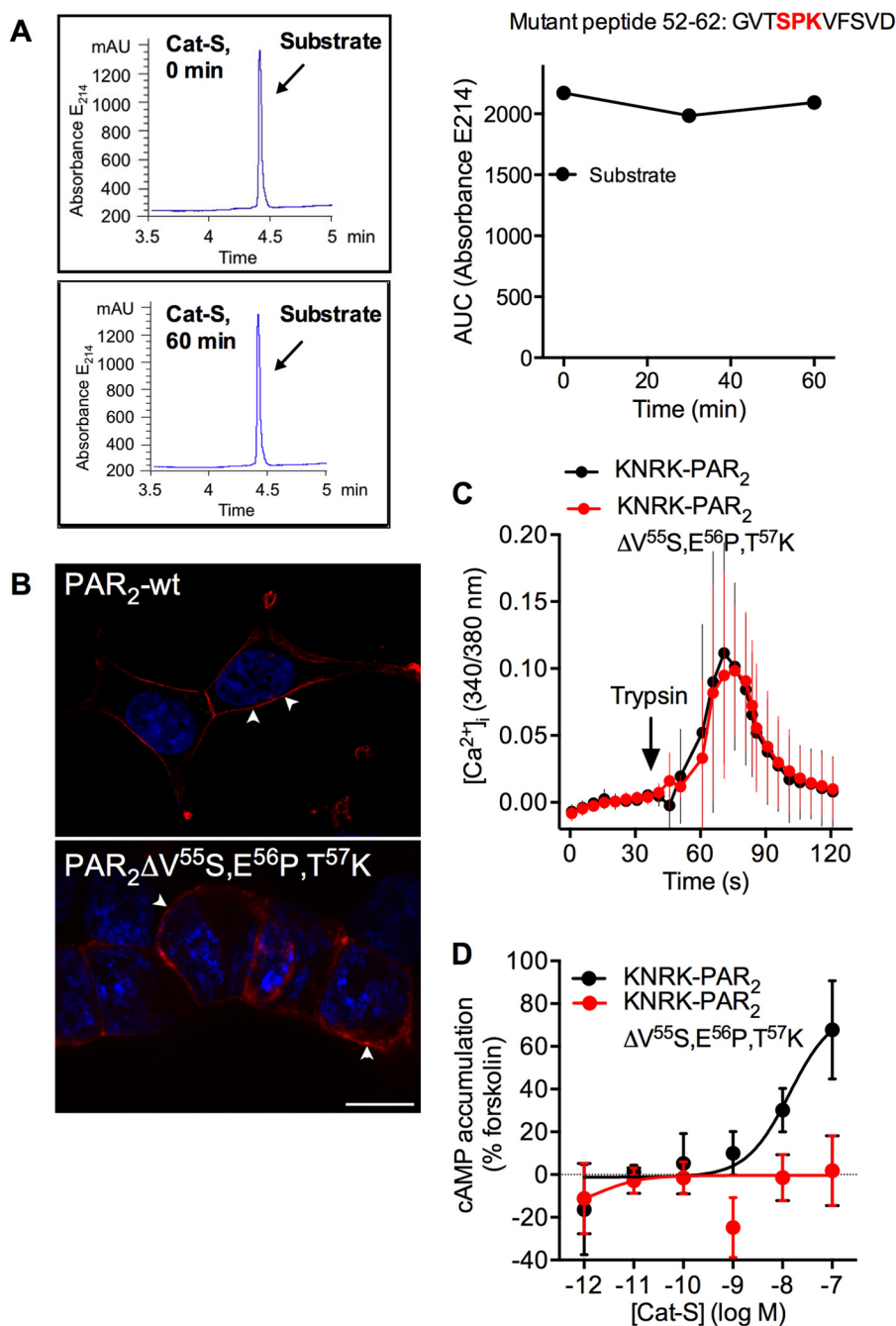
FIGURE 8. **Requirement of PAR₂ cleavage for activation by Cat-S.** *A*, Cat-S degradation of PAR₂ ^{52}GVTSPKVFSVD^{62}. HPLC traces (*left*) show elution of the substrate after incubation with Cat-S for 0 min or 60 min. Time course (*right*) shows the kinetics of substrate degradation and product formation. In *red* are the residues replaced from the wild-type sequence. *B*, localization of wild-type PAR₂ and PAR₂ΔV^{55}S/E^{56}P/T^{57}K expressed in HEK293 cells by immunofluorescence, using antibody to intracellular C-terminal HA11 epitope, and confocal microscopy. Scale bar 10 μm. *C*, trypsin (100 nM)-evoked Ca²⁺ signals in individual KNRK cells transiently expressing wild-type PAR₂ or PAR₂ΔV^{55}S/E^{56}P/T^{57}K. Cells were co-transfected with GFP for identification. *D*, Cat-S-evoked cAMP formation in KNRK cells transiently expressing wild-type PAR₂ and PAR₂ΔV^{55}S/E^{56}P/T^{57}K. Triplicate measurements of n = 3–4 experiments.

ment of TRPV4-expressing oocytes with trypsin, Cat-S or Cat-S AP did not alter the TRPV4 response (Fig. 9, *B–D*). In vehicle-treated oocytes expressing TRPV4 plus PAR₂, the response to GSK1016790A was the same as in oocytes expressing TRPV4 alone (Fig. 9*A*). Pre-incubation of oocytes expressing TRPV4 plus PAR₂ with trypsin, Cat-S or Cat-S AP for 5 min amplified the response to GSK1016790A, indicating TRPV4 sensitization (Fig. 9, *B–D*). Compared with the response in oocytes expressing TRPV4, the responses of oocytes expressing TRPV4 plus PAR₂ was amplified by ~8-fold after trypsin and ~5-fold after

Cat-S and Cat-S AP (Fig. 9*E*). Thus, Cat-S induces PAR₂-dependent sensitization of TRPV4.

We similarly examined whether Cat-S can sensitize TRPV4 stably expressed in HEK293 cells. HEK-TRPV4 cells were incubated with vehicle (control), Cat-S (100 nM) or trypsin (100 nM) for 5 min and were then challenged with GSK1016790A (100 pM). In vehicle-treated cells, GSK1016790A caused a gradual and sustained increase in [Ca²⁺]$_i$, consistent with TRPV4 activation (Fig. 9*F*). Trypsin, but not Cat-S, increased [Ca²⁺]$_i$, and preincubation with both proteases resulted in a ~3-fold
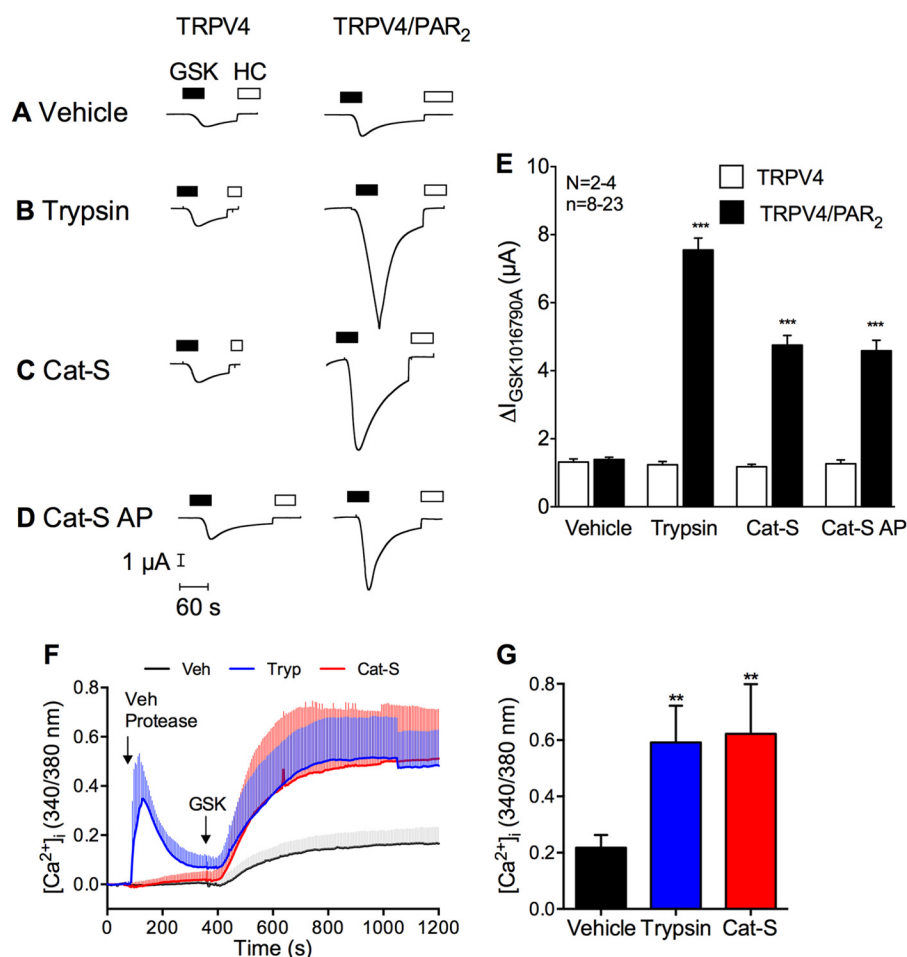
FIGURE 9. **Cat-S- and PAR$_2$-dependent sensitization of TRPV4.** *A–E*, *Xenopus laevis* oocytes expressing TRPV4 alone or TRPV4 plus PAR$_2$ were pre-incubated with vehicle (control, *A*), trypsin (8 nM, *B*), Cat-S (1 µM, *C*), or Cat-S AP (50 µM, *D*) for 5 min. After pre-incubation, TRPV4 was activated and then inhibited with GSK1016790A (GSK, *closed bars*) (50 nM) and HC067047 (HC, *open bars*) (100 nM), respectively. *A–D*, representative whole-cell currents. *E*, mean $\Delta I_{GSK1016790A}$ values of pooled experiments. *n* indicates number of individual oocytes studied. *N* indicates the number of batches of oocytes. ***, $p < 0.001$ compared with vehicle. *F* and *G*, HEK-TRPV4 cells were incubated with vehicle (control), trypsin (*Tryp.*, 100 nM) or Cat-S (100 nM) for 5 min, and then challenged with GSK1016790A (GSK, 100 pM). Changes in $[Ca^{2+}]_i$ were measured in individual cells using Fura-2/AM. *F*, effects of proteases and GSK1016790A on $[Ca^{2+}]_i$. *G*, maximal responses to GSK1016790A. *n* = 3 experiments, >250 cells per data point. **, $p < 0.01$ compared with vehicle.

increase in the maximal response to GSK1016790A (Fig. 9, *F* and *G*). Thus, Cat-S sensitizes TRPV4 in HEK293 cells as well as in oocytes.

Cat-S Is a Biased Agonist of PAR$_2$ in DRG Neurons—PAR$_2$ is expressed by nociceptive neurons, where activation induces neurogenic inflammation (10) and pain (32). To determine whether Cat-S is a biased agonist of PAR$_2$ in nociceptive neurons, we challenged mouse DRG neurons with trypsin or Cat-S (100 nM) and measured cAMP accumulation, ERK1/2 activation and $[Ca^{2+}]_i$. Trypsin and Cat-S stimulated cAMP accumulation to a similar extent that was maximal after 30 min (Fig. 10*A*). Trypsin but not Cat-S stimulated ERK1/2 activation, which was maximal after 20 min (Fig. 10*B*). Trypsin stimulated an increase in $[Ca^{2+}]_i$ in 24.7 $\pm$ 7.1% and Cat-S stimulated an increase in $[Ca^{2+}]_i$ in 40.4 $\pm$ 10.7% of small diameter neurons from wild-type mice, similar to the proportion of neurons that responded to capsaicin (41.0 $\pm$ 4.8%) (Fig. 10, *C*, *D*, *G*). In the absence of extracellular Ca^{2+} ions, the response to trypsin was diminished but not abolished (Fig. 10, *C* and *E*), whereas the response to Cat-S was undetectable (Fig. 10, *D*, *F*). Significantly fewer neurons from *par2$^{-/-}$* or *trpv4$^{-/-}$* mice responded to

Cat-S with a detectable increase in $[Ca^{2+}]_i$ (wild-type 40.4 $\pm$ 10.7%, *par2$^{-/-}$* 14.3 $\pm$ 0.5%, *trpv4$^{-/-}$* 4.7 $\pm$ 2.5% of small diameter neurons, $p < 0.05$ to wild-type) (Fig. 10*H*). The TRPV4 antagonist HC067047 inhibited Cat-S responses of neurons from wild-type mice (Fig. 10*H*). The PKA inhibitor PKI and the adenylyl cyclase inhibitor SQ22536 both suppressed Cat-S responses of neurons from wild-type mice (Fig. 10*I*). These results suggest that the Cat-S-evoked increase in $[Ca^{2+}]_i$ depends on activation of PAR$_2$ and entails TRPV4-dependent influx of Ca^{2+} ions, rather than mobilization of intracellular Ca^{2+} stores. They are consistent with activation of TRPV4 in neurons *via* biased signaling of the PAR$_2$/adenylyl cyclase/cAMP/PKA pathway. The residual Ca^{2+} responses in neurons from *par2$^{-/-}$* and *trpv4$^{-/-}$* mice occur by unknown mechanisms, possibly involving other PARs and TRP channels. As in HEK and KNRK cell lines, Cat-S preferentially signals *via* cAMP in DRG neurons.

Cat-S Induces a PKA-induced Hyperexcitability of Nociceptive Neurons—Cat-S induces hyperexcitability of nociceptive neurons from wild-type but not *par$_2$$^{-/-}$* mice by unknown mechanisms (5). To determine whether PAR$_2$ biased signaling

FIGURE 10. **Cat-S biased signaling in DRG neurons.** The effects of trypsin (*Tryp.*, 100 nM) and Cat-S (100 nM) on cAMP accumulation (*A*), ERK1/2 activation (*B*) and $[Ca^{2+}]_i$ (*C–I*) were measured in DRG neurons. *C–F*, effects of trypsin and Cat-S on $[Ca^{2+}]_i$. *E* and *F*, assays in Ca^{2+}-free extracellular fluid. *G*, proportion of small diameter neurons responding to trypsin, Cat-S or capsaicin (Cap.). *H*, proportion of small diameter neurons responding to Cat-S in neurons from wild-type (WT) mice, *par2$^{-/-}$* or *trpv4$^{-/-}$* mice, or wild-type mice treated with the TRPV4 antagonist HC067047. *I*, proportion of small diameter neurons responding to Cat-S in neurons from wild-type mice treated with vehicle (*Veh.*) the PKA inhibitor PKI or the adenylyl cyclase inhibitor SQ22536. *A–C*, *H*, *I*, $n = 4$–6 mice. *C–F*, records from 15–20 individual neurons. $p < 0.05$ compared with wild-type or vehicle.

accounts for this effect, we examined the actions of inhibitors of PKA (PKI, H-89), adenylyl cyclase (SQ22536), and PKC (GF-109201X) on Cat-S-evoked neuronal hyperexcitability. We incubated small diameter mouse DRG neurons with Cat-S (100 nM) or vehicle (control) for 60 min, and then measured the rheobase (minimum current to generate an action potential) and the action potential discharge at twice rheobase by patch-clamp recording to assess neuronal hyperexcitability. Cat-S decreased the rheobase (vehicle, 69.8 ± 2.8 pA, $n = 57$ neurons; Cat-S, 39.6 ± 2.8 pA, $n = 55$ neurons; $p < 0.0001$) and increased the frequency of action potential discharge (vehicle, 1.21 ± 0.06; Cat-S, 1.98 ± 0.13; $p < 0.0001$), indicating hyperexcitability (Fig. 11). Inhibition of PKA with PKI or H-89 abolished the effects of Cat-S on rheobase and action potential firing (Fig. 11, *A–C*). Inhibition of adenylyl cyclase with SQ22536 inhibited the effects of Cat-S on rheobase (Fig. 11*D*). In contrast, inhibition of PKC with GF-109203X had no effect on Cat-S-evoked changes in rheobase or action potential discharge (Fig. 11*E*). None of the inhibitors affected the rheobase of action potential

firing of vehicle-treated neurons. Thus, three distinct inhibitors (PKI, H-89, SQ22526) of the adenylyl cyclase/cAMP/PKA pathway blocked the effects of Cat-S on nociceptor hyperexcitability. These results suggest that Cat-S evokes PAR$_2$-dependent hyperexcitability of nociceptive neurons *via* biased activation of adenylyl cyclase/cAMP/PKA but not PKC signaling pathways.

Cat-S Induces PAR$_2$- and TRPV4-dependent Inflammation and Pain—Intraplantar injection of trypsin or trypsin-revealed AP induces neurogenic inflammation and hyperalgesia by PAR$_2$- and TRP-dependent mechanisms (10, 27, 28, 32). TRPV4 agonists also cause neurogenic inflammation and mechanical hyperalgesia (28, 52). To examine whether Cat-S causes inflammation and pain by similar mechanisms, we made intraplantar injections of Cat-S (1.4–14 μM, 10 μl) to wild-type, *par$_2$$^{-/-}$*, and *trpv4$^{-/-}$* mice. We assessed mechanical hyperalgesia using calibrated von Frey filaments and inflammatory edema using calipers to measure paw thickness. In wild-type mice, Cat-S caused a dose-related decrease in the filament stiffness required to elicit paw withdrawal that was

A

Rheobase   2 X Rheobase

Control

50 mV
250 ms

70 pA   140 pA

Cat-S

40 pA   80 pA

Cat-S
+ PKI

60 pA   120 pA

B. Cat-S + PKI

C. Cat-S + H-89

D. Cat-S + SQ22536

E. Cat-S + GF109203X
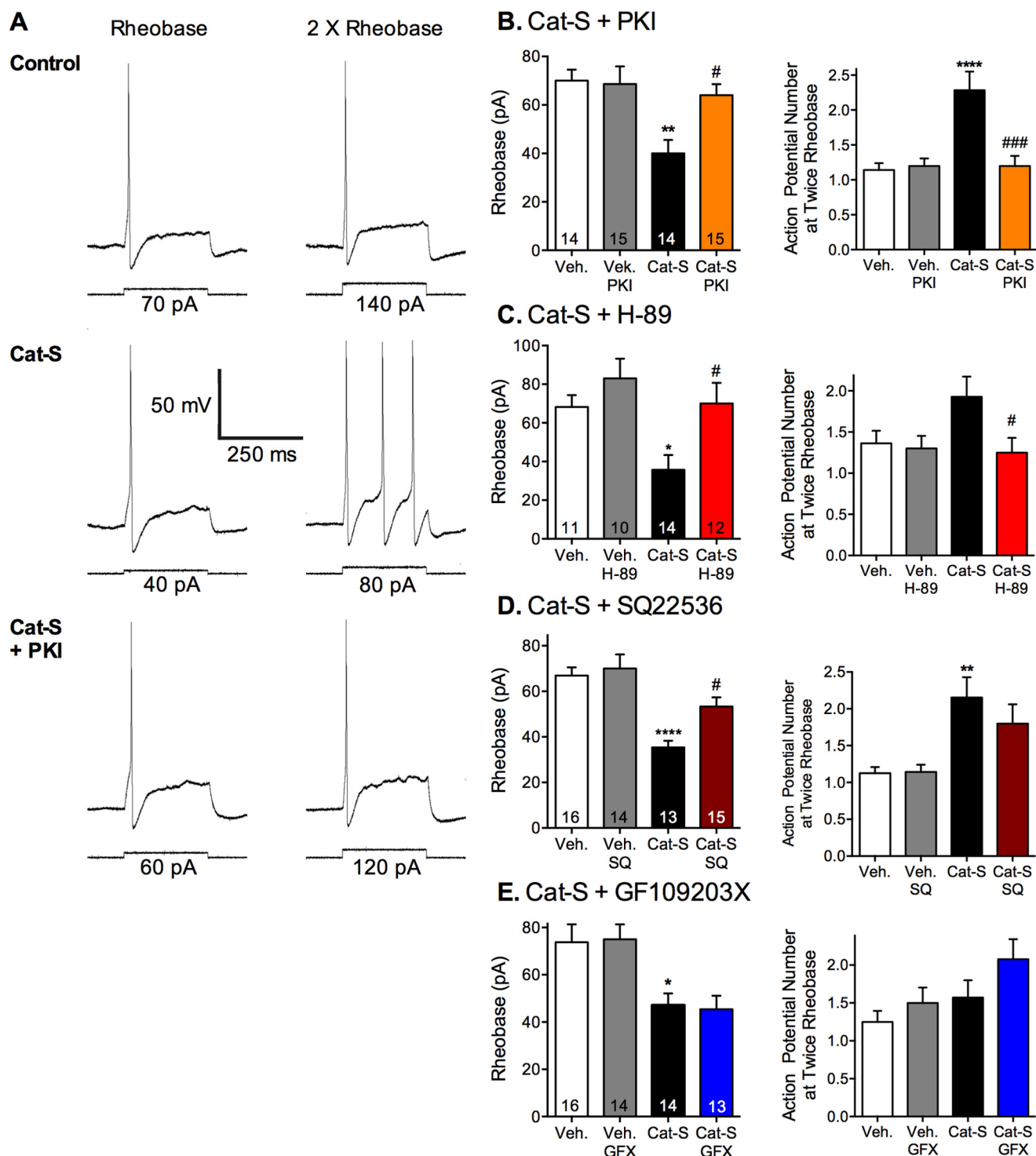
FIGURE 11. **Cat-S-induced and adenylyl cyclase/PKA-dependent hyperexcitability of nociceptive neurons.** Small diameter DRG neurons were preincubated with vehicle (control) or Cat-S (100 nM) for 60 min. Rheobase and frequency of action potential discharge at twice rheobase were measured to assess hyperexcitability. In some experiments, neurons were pre-incubated with PKI (10 μM), H-89 (10 μM), SQ22536 (SQ, 20 μM), or GF-109203X (GFX, 10 μM). *A*, representative traces of rheobase and action potential discharge at twice rheobase. *B–E*, pooled results showing rheobase (*left panels*) and action potential discharge at twice rheobase (*right panels*) or neurons treated with vehicle or Cat-S with PKI (*B*), H-89 (*C*), SQ22536 (*D*), or GF-109203X (*F*). Numbers of studied neurons are shown in *bars*. *, $p < 0.05$; **, $p < 0.01$; ****, $p < 0.0001$ Cat-S compared with vehicle; #, $p < 0.05$; ###, $p < 0.001$ Cat-S plus inhibitor compared with Cat-S.

maximal after 1 h and sustained for at least 4 h, indicative of mechanical hyperalgesia (Fig. 12, *A* and *B*). Cat-S (14 μM, 10 μl) also caused edema that was maximal at 1 h and maintained for 4 h, indicative of edema (Fig. 12*C*). PAR$_2$ deletion inhibited Cat-S-induced mechanical hyperalgesia and edema at all

time points, whereas TRPV4 deletion attenuated paw edema after 2 h but did not prevent the hyperalgesia (Fig. 12, *B* and *C*). Thus, Cat-S evokes pain and inflammation by a PAR$_2$-dependnet process, and TRPV4 contributes to the sustained Cat-S-induced inflammation.
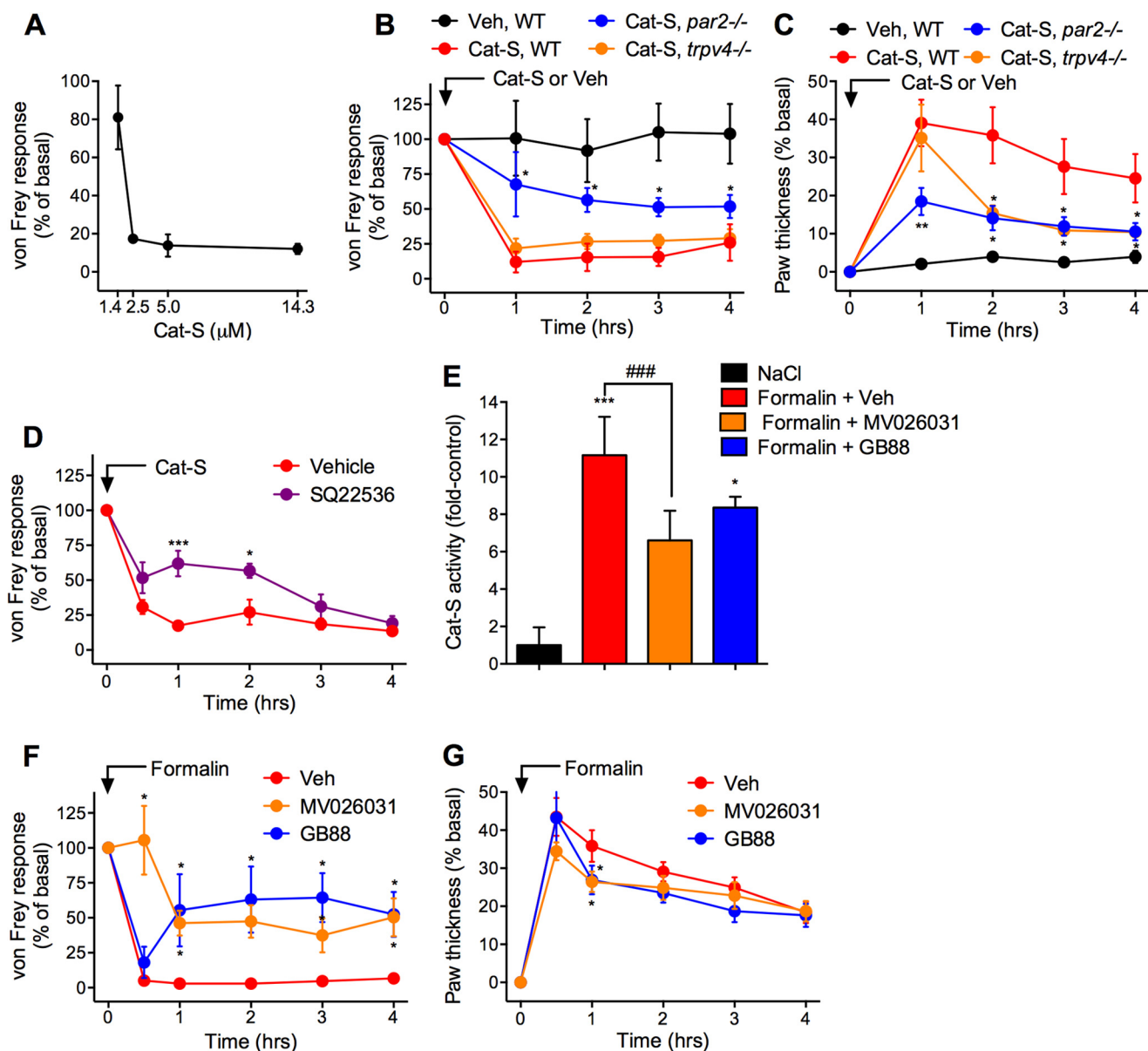
FIGURE 12. **Contributions of Cat-S, PAR₂ and TRPV4 to pain and inflammation.** *A–C*, Cat-S (1.4–14 μM, 10 μl) or vehicle (*Veh*, control) was administered by intraplantar injection to wild-type (*WT*), *par2⁻/⁻* and *trpv4⁻/⁻* mice. Mechanical hyperalgesia was measured using von Frey filaments (*A, B*) and edema was assessed by measurement of paw diameter with calipers (*C*). *A*, effects of graded Cat-S doses on mechanical hyperalgesia at 1 h. *B* and *C*, effects of 14 μg Cat-S. *, $p < 0.05$; ***, $p < 0.001$ compared with vehicle. *D*, effects of Cat-S (2.5 μM) on mechanical hyperalgesia in mice pre-treated with SQ22536 or vehicle. *F* and *G*, formalin (4%, 10 μl) was administered by intraplantar injection to wild-type mice pre-treated with MV026031, GB88 or vehicle (*Veh*, control). *E*, at 4 h after formalin injection, the paws were removed for Cat-S activity assays. *, $p < 0.05$; ***, $p < 0.001$ to NaCl; ###, $p < 0.001$ to vehicle. *F*, mechanical hyperalgesia in formalin-treated mice. *G*, edema in formalin-treated mice. *, $p < 0.05$ compared with vehicle. $n = 6$–8 mice.

To determine whether Cat-S causes mechanical hyperalgesia *via* biased agonism of PAR₂, we examined the effects of inhibiting the adenylyl cyclase/PKA pathway on Cat-S-evoked pain. Wild-type mice received an intraplantar injection of the adenylyl cyclase inhibitor SQ22536 or vehicle, followed by Cat-S (2.5 μM, 10 μl). In vehicle-treated mice, Cat-S caused a sustained mechanical hyperalgesia (Fig. 11*D*). SQ22536 inhibited Cat-S-evoked hyperalgesia at 1 and 2 h (Fig. 12*D*). These results suggest that Cat-S induces mechanical hyperalgesia *via* the adenylyl cyclase pathway, and are consistent with the capacity of Cat-S to cause hyperexcitability of nociceptive neurons by an adenylyl cyclase- and PKA-dependent process (Fig. 11). It was not possible to examine directly the contribution of PKA to

Cat-S-evoked pain, since the PKA inhibitor WIPTIDE, which is commonly used to study the role of PKA in pain *in vivo*, is a peptide and would be likely degraded by Cat-S.

To determine whether endogenous Cat-S contributes to pain and inflammation, we made intraplantar injections to mice of formalin, which causes PAR₂-dependent hyperalgesia (32). Intraplantar formalin (4%, 10 μl) induced a 12-fold increase in Cat-S activity in the paw tissue, as determined using the Cat-S substrate acetyl-KQKLR-AMC (Fig. 12*E*). Pre-treatment of mice with the Cat-S inhibitor MV026031 (50 mg/kg p.o.) 2 h before formalin injection suppressed formalin-induced activation of Cat-S, which confirms the effectiveness of this inhibitor at the dose given *in vivo*. Formalin induced the expected rapid

and sustained mechanical hyperalgesia and edema (Fig. 12, *F* and *G*). MV026031 inhibited formalin-induced mechanical hyperalgesia at all times and suppressed edema at 1 h (Fig. 12, *F* and *G*). Pre-treatment with the PAR$_2$ antagonist GB88 (10 mg/kg p.o.) inhibited mechanical hyperalgesia after 1 h and also suppressed edema at 1 h (Fig. 12, *F* and *G*). These results reveal a role for endogenous Cat-S and PAR$_2$ in formalin-induced inflammation and pain.

DISCUSSION

We report a new mechanism by which Cat-S activates PAR$_2$ and TRPV4 to cause inflammation and pain. Our major finding is that Cat-S is a biased agonist of PAR$_2$. By cleaving PAR$_2$ at a unique site ($E^{56} \downarrow T^{57}$), which is distal to the canonical tethered ligand that is exposed by trypsin cleavage, Cat-S reveals a distinct tethered ligand domain. Cat-S cleavage stabilizes conformations of PAR$_2$ that signal by mechanisms that are distinctly different from those activated by trypsin. After cleavage by Cat-S, PAR$_2$ couples to Gαs, leading to the formation of cAMP. In contrast to trypsin-activated PAR$_2$, Cat-S cleavage fails to mobilize intracellular Ca^{2+}, activate ERK1/2, recruit β-arrestins or cause receptor endocytosis. Cat-S-cleaved PAR$_2$ sensitizes TRPV4 and causes hyperexcitability of nociceptive neurons by an adenylyl cyclase- and PKA-mediated pathway. The intraplantar administration of Cat-S causes sustained mechanical hyperalgesia and inflammatory edema in mice by PAR$_2$-, TRPV4-, and adenylyl cyclase-dependent mechanisms. Intraplantar formalin, which induces sustained inflammation and pain, activates Cat-S, and a Cat-S inhibitor and PAR$_2$ antagonist both suppress formalin-induced inflammation and pain. Given that Cat-S is activated and secreted in inflammatory diseases, our findings indicate that antagonists of Cat-S, PAR$_2$ and TRPV4 may be useful treatments for inflammation and pain.

Cat-S Is a Biased Agonist of PAR$_2$—We have identified a new mechanism by which Cat-S activates PAR$_2$. The established mechanism by which serine proteases such as trypsin, tryptase and kallikreins activate PAR$_2$ involves hydrolysis of the $R^{36} \downarrow S^{37}$ bond and exposure of the tethered ligand domain ^{37}SLIGKV, which binds to and activates the cleaved receptor. By incubating synthetic fragments of the extracellular N terminus of PAR$_2$ with Cat-S, we identified that Cat-S cleaves within the N terminus of PAR$_2$ at a single major site: $E^{56} \downarrow T^{57}$. In experiments in HEK293 cells expressing PAR$_2$ with N-terminal Flag and C-terminal HA11 epitopes, we observed that Cat-S removed the extracellular Flag epitope, which indicates that Cat-S can cleave intact PAR$_2$ at the cell surface as well as receptor fragments. To ascertain the importance of cleavage at the $E^{56} \downarrow T^{57}$ for Cat-S activation of PAR$_2$, we studied the capacity of Cat-S to cleave and activate a mutant receptor in which the P2, P1 and P1′ positions were replaced: $V^{55} \rightarrow S$, $E^{56} \rightarrow P$, and $T^{57} \rightarrow K$. Cat-S did not cleave a fragment with these substitutions (^{52}GVTSPKVFSVD^{62}), and Cat-S was unable to stimulate formation of cAMP in KNRK cells expressing PAR$_2\Delta V^{55}$S/ E^{56}P/T^{57}K. PAR$_2\Delta V^{55}$S/E^{56}P/T^{57}K was normally localized at the plasma membrane and trypsin stimulated Ca^{2+} signaling in KNRK-PAR$_2\Delta V^{55}$S/E^{56}P/T^{57}K cells, which indicate that membrane trafficking and trypsin activation are unaffected by these mutations. Identification of $E^{56} \downarrow T^{57}$ as the major site at which

Cat-S cleaves within the N terminus of PAR$_2$ is consistent with the known requirements for Cat-S substrate recognition (56, 57). Aliphatic residues at the P2 position, including valine and leucine, direct Cat-S selectivity. The P1 position can tolerate several other residues including glycine, lysine, glutamic acid, glutamine, tyrosine, and alanine, while other positions contribute little to Cat-S recognition. We identified a single site of Cat-S cleavage, despite numerous aliphatic residues within the PAR$_2$ N terminus, including eight valine residues. Thus, the selectivity with which Cat-S cleaves PAR$_2$ probably relies on a series of mutual interactions from numerous sites, which requires future study. In addition to the $E^{56} \downarrow T^{57}$ site, Cat-S can also cleave PAR$_2$ more proximally at $G^{41} \downarrow K^{42}$ (58). However, this study did not assess whether Cat-S cleaves PAR$_2$ at the site that we have identified.

The Cat-S cleavage site ($E^{56} \downarrow T^{57}$) is distal to the trypsin cleavage site ($R^{36} \downarrow S^{37}$). We observed that pre-incubation with Cat-S attenuated trypsin-evoked Ca^{2+} signaling in HEK293 cells and trypsin-induced activation of calcium-activated chloride channels in oocytes. These findings are consistent with the proposal that Cat-S, by removing the trypsin cleavage site, disarms PAR$_2$ for trypsin activation. Similarly, neutrophil elastase cleaves PAR$_2$ at $S^{68} \downarrow V^{69}$, which also prevents trypsin-stimulated PAR$_2$ signaling (33, 34). The patho-physiological relevance of these mechanisms of PAR$_2$ disarming is uncertain.

We found that Cat-S-activated PAR$_2$ signals by mechanisms that are distinctly different from those arising from trypsin-activated PAR$_2$. We examined PAR$_2$ coupling to heterotrimeric G proteins using BRET. Proteases stimulated distinct BRET signals between PAR$_2$-RLuc8 and Gγ2-Venus. Cat-S induced a sustained increase in BRET only in the presence of overexpressed Gαs, whereas trypsin induced a sustained increase in BRET in the presence of Gαq and a transient decrease in BRET in the presence of Gαs. Similar differences in coupling between PAR$_2$ and different G proteins have been observed in Cos-7 cells, where trypsin induces a sustained signal between PAR$_2$ and Gα12, but a rapid and transient signal between PAR$_2$ and Gαi (59). The rapid decline in BRET signal may due to receptor desensitization or dissociation of G$\beta\gamma$ dimer from the complex. The reason for the differences in trypsin- and Cat-S-induced BRET in cells expressing Gαs is unclear. One possible explanation is that Cat-S and trypsin cleave PAR$_2$ at distinct sites, and that Cat-S cleavage results in a higher affinity or more stable association between the tethered ligand and the receptor. Alternatively, the trypsin- and Cat-S cleaved receptor may adopt distinct conformations that interact differently with G proteins. Although the structural determinants for PAR$_2$ coupling to Gαq and Gαs remain to be identified, our results suggest that proximal regions of PAR$_2$ that are revealed by trypsin cleavage mediate Gαq coupling, whereas distal regions exposed by Cat-S or trypsin cleavage mediate Gαs coupling.

The observations that Cat-S-activated PAR$_2$ couples to Gαs alone, whereas trypsin-activated PAR$_2$ couples to both Gαs and Gαq, are consistent with the capacity of Cat-S to generate cAMP but not to mobilize intracellular Ca^{2+}, whereas trypsin induces both signals. Trypsin, but not Cat-S, also activated ERK1/2, recruited β-arrestins and caused PAR$_2$ endocytosis. The inability of Cat-S-cleaved PAR$_2$ to activate ERK1/2 and to

internalize agrees with the lack of interactions with β-arrestins, which mediate PAR$_2$ ERK1/2 signaling (36) and endocytosis (47). The Cat-S inhibitor MV026031 prevented Cat-S induced formation of cAMP in HEK-PAR$_2$ cells, indicating a requirement for enzymatic activity. Cat-S-induced cAMP formation is attributable to cleavage and activation of PAR$_2$ since the PAR$_2$ antagonist GB88 (55) prevented Cat-S stimulation of cAMP generation in HEK-PAR$_2$ cells, and because Cat-S stimulated cAMP formation in KNRK cells expressing wild-type PAR$_2$ but not the cleavage-resistant mutant PAR$_2\Delta$V^{55}S/E^{56}P/T^{57}K.

A synthetic peptide corresponding to the first 10 residues distal to the Cat-S cleavage site (^{57}TVFSVDEFSA, Cat-S AP) induced Gαs-dependent BRET signals between PAR$_2$-RLuc8 and Gγ2-Venus, and stimulated cAMP formation in KNRK-PAR$_2$ cells but not in KNRK-VC cells. Whereas Cat-S and trypsin increased Gαs-dependent BRET signals, Cat-S AP caused a large and sustained decrease in BRET. The reason for this difference is unknown, but the results suggest that the receptor adopts distinctly different conformations after cleavage by Cat-S or activation by Cat-S AP. Our results indicate that Cat-S, like trypsin, reveals a tethered ligand that binds to and activates the cleaved receptor. After trypsin cleavage, the tethered ligand interacts with domains in the second extracellular loop of PAR$_2$ (60). Further studies are required to ascertain whether the Cat-S-revealed tethered ligand similarly activates PAR$_2$ and to identify key residues that are required for such interactions. However, PAR$_2$ cleavage may also be sufficient to induce conformational changes that result in receptor activation without tethered ligand binding. In case of elastase, synthetic peptides that mimic a potential tethered ligand are unable to activate PAR$_2$, possibly because the elastase cleavage site (S^{68} $\downarrow$ V^{69}) is close to the first transmembrane domain (34). In contrast, elastase can activate PAR$_1$ by a tethered ligand mechanism (37). A recent report suggests that Cat-S can cleave PAR$_2$ at G^{41} $\downarrow$ K^{42} to reveals a the tethered ligand ^{42}KVDGTS, which, like the trypsin-exposed AP SLIGRL, stimulates Ca^{2+} signaling in HeLa cells, albeit with reduced potency (58). However, we found no evidence that Cat-S induced mobilization of intracellular Ca^{2+} in KNRK or HEK cells expressing PAR$_2$, but instead observed that Cat-S stimulates a TRPV4-dependent influx of extracellular Ca^{2+} ions in nociceptive neurons.

Biased agonism, by which different endogenous ligands or drugs induce distinct conformations of the same GPCR leading to diverse signaling patterns and outcomes, is an emerging theme in the GPCR field (35). However, in contrast to most instances, where biased agonists activate the same set of signaling pathways but with differential potencies, Cat-S activated PAR$_2$ by a single mechanism, Gαs-dependent formation of cAMP, and was completely inactive in all other pathways at any tested concentration. Neutrophil elastase is another biased agonist of PAR$_2$, since elastase stimulates PAR$_2$-dependent activation of ERK1/2 by a Rho-kinase dependent but β-arrestin-independent pathway (34). The observation that Cat-S- and elastase-activated PAR$_2$ neither interacts with β-arrestins nor internalizes has implications for PAR$_2$ desensitization and down-regulation, which involve β-arrestin-mediated uncoupling of PAR$_2$ from heterotrimeric G-proteins and PAR$_2$ endocytosis and lysosomal degradation (36, 47, 54). We found that

Cat-S-activated PAR$_2$ remained at the cell surface, and that Cat-S induced sustained Gαs-dependent PAR$_2$-RLuc8 and Gγ2-Venus BRET. These findings suggest that Cat-S could induce sustained signals from PAR$_2$ at the plasma membrane. Further studies are necessary to elucidate the importance of such signals and to investigate the fate of PAR$_2$ after cleavage by proteases that fail to recruit β-arrestins and cause receptor endocytosis.

Patho-physiological Importance of Cat-S PAR$_2$ Signaling— Our results show that Cat-S-activated PAR$_2$ couples to signaling pathways that sensitize and activate TRPV4 and cause inflammation and pain. We have thus identified a patho-physiologically relevant outcome of Cat-S biased agonism of PAR$_2$.

We observed that pre-incubation with Cat-S and Cat-S AP strongly (5-fold) amplified TRPV4 currents in oocytes co-expressing PAR$_2$ and TRPV4, but did not affect TRPV4 currents in oocytes expressing TRPV4 alone. Cat-S similarly amplified TRPV4 Ca^{2+} signals in HEK-TRPV4 cells. Thus, Cat-S-activated PAR$_2$ can sensitize TRPV4. Our results suggest that Cat-S is a biased agonist of PAR$_2$ in nociceptive neurons that control pain and neurogenic inflammation. Both Cat-S and trypsin stimulated cAMP formation in DRG cultures, whereas trypsin alone stimulated ERK1/2 activation. These results are consistent with observations in KNRK and HEK cells. Although both Cat-S and trypsin increased $[Ca^{2+}]_i$ in DRG neurons, the response to Cat-S was prevented by removal of extracellular Ca^{2+}, whereas the response to trypsin was only slightly reduced. Thus, Cat-S-activated PAR$_2$ couples to mechanisms that induce Ca^{2+} influx in neurons but not mobilization of intracellular Ca^{2+} stores. PAR$_2$-deletion or deletion or antagonism of TRPV4 markedly reduced Cat-S-evoked Ca^{2+} signals in neurons, which indicates that Cat-S causes a PAR$_2$-dependent activation of TRPV4, leading to Ca^{2+} influx. The adenylyl cyclase inhibitor SQ22536 and the PKA inhibitor PKI both suppressed Cat-S Ca^{2+} signals, suggesting a major role for the PAR$_2$ biased adenylyl cyclase/cAMP/PKA signaling pathway in TRPV4 activation. PKA and PKC play a major role in sensitizing TRPV4 through phosphorylation of serine and threonine residues, including S^{824} in the case of PKA, and assembly of a complex with the scaffolding protein AKAP79 (61). After activation by trypsin or trypsin AP, PAR$_2$ sensitizes and activates TRPV4 by several mechanisms, which include PKC- and tyrosine kinase-dependent processes, as well as formation of arachidonic acid metabolites that are TRPV4 agonists (28, 29). Thus, multiple proteases that can activate PAR$_2$ by distinct mechanisms are capable of sensitizing TRP channels by divergent signaling processes.

We have previously show that Cat-S causes hyperexcitability of nociceptive neurons in wild-type but not $par_2^{-/-}$ mice, but by unknown signaling pathways (5). In the present study we found that Cat-S also reduced the rheobase and increased action potential discharge, confirming hyperexcitability. Pharmacological inhibitors of adenylyl cyclase (SQ22536) and two different PKA inhibitors (PKI, H-89) suppressed this sensitization, which further implicates PAR$_2$ biased signaling by the Gαs, adenylyl cyclase, cAMP and PKA pathway in this process.

Intraplantar injection of Cat-S to mice caused sustained inflammatory edema and mechanical hyperalgesia. Deletion of

par$_2$ strongly inhibited inflammation and pain at all time points, whereas deletion of *trpv4* inhibited only the later stages of inflammation, consistent with the requirement of TRPV4 for sustained inflammatory signaling of PAR$_2$ (29). The residual inflammation and pain observed in *par$_2$$^{-/-}$* mice may be mediated by Cat-S activation of other PARs, which may also explain the small PAR$_2$-independent Ca^{2+} signals to Cat-S in DRG neurons from *par$_2$$^{-/-}$* mice. Other proteases (trypsin 4) can also cause inflammation by activating both PAR$_1$ and PAR$_2$ (15). Cat-S induced inflammation and pain could also be caused by sensitization and activation of other TRP channels, since PAR$_2$ can sensitize TRPV1 and TRPA1 and induce neurogenic inflammation and pain (27, 31). The finding that Cat-S causes PAR$_2$-dependent inflammation and pain is consistent with our previous report that Cat-S causes visceral pain, which required expression of PAR$_2$ (5). Inhibition of adenylyl cyclase strongly inhibited Cat-S-evoked mechanical hyperalgesia, which implicates PAR$_2$ biased signaling. Antagonism of Cat-S and PAR$_2$ suppressed formalin-induced pain and inflammation, which suggests that endogenous Cat-S can activate PAR$_2$ to cause algesic and inflammatory signals. The intraplantar injection of formalin resulted in Cat-S activation, possibly due to the infiltration of macrophages that are a major source of Cat-S. The Cat-S inhibitor MV026031 suppressed Cat-S activity in tissues and blocked formalin-induced mechanical hyperalgesia and inflammation, confirming the importance of endogenous Cat-S. In agreement with the report that PAR$_2$ deletion attenuates formalin-induced pain (32), we observed that the PAR$_2$ antagonist GB88 inhibited the algesic and inflammatory actions of formalin. GB88 also blocks the inflammatory effects of PAR$_2$ agonists and of carrageenan (62).

Our finding that Cat-S is a biased agonist of PAR$_2$- and TRPV4-dependent inflammation and pain has implications for the mechanism and treatment of disease. Cat-S is activated in DRG macrophages (6) and spinal microglial cells (7) after nerve injury. Cat-S from microglial cells liberates fractalkine from spinal neurons, which activates CX3CR1 on microglial cells to trigger inflammatory signals that contribute to central sensitization of pain (1, 7, 8). Whether Cat-S can activate PAR$_2$ on the central projections of primary sensory neurons within the dorsal horn to cause pain remains to be investigated. Cat-S is also activated in inflammatory diseases including rheumatoid arthritis (4) and colitis (5). Given the established contributions of PAR$_2$ and TRPV4 to arthritis (63) and colitis (30, 64, 65), antagonists of Cat-S, PAR$_2$, and TRPV4 may be valuable treatments for these and other inflammatory diseases.

REFERENCES

1. Clark, A. K., and Malcangio, M. (2012) Microglial signalling mechanisms: Cathepsin S and Fractalkine. *Exp. Neurol.* **234,** 283–292
2. Clark, A. K., Wodarski, R., Guida, F., Sasso, O., and Malcangio, M. (2010) Cathepsin S release from primary cultured microglia is regulated by the P2X7 receptor. *Glia* **58,** 1710–1726
3. Liuzzo, J. P., Petanceska, S. S., Moscatelli, D., and Devi, L. A. (1999) Inflammatory mediators regulate cathepsin S in macrophages and microglia: A role in attenuating heparan sulfate interactions. *Mol. Med.* **5,** 320–333
4. Pozgan, U., Caglic, D., Rozman, B., Nagase, H., Turk, V., and Turk, B. (2010) Expression and activity profiling of selected cysteine cathepsins and matrix metalloproteinases in synovial fluids from patients with rheumatoid arthritis and osteoarthritis. *Biol. Chem.* **391,** 571–579
5. Cattaruzza, F., Lyo, V., Jones, E., Pham, D., Hawkins, J., Kirkwood, K., Valdez-Morales, E., Ibeakanma, C., Vanner, S. J., Bogyo, M., and Bunnett, N. W. (2011) Cathepsin S is activated during colitis and causes visceral hyperalgesia by a PAR2-dependent mechanism in mice. *Gastroenterology* **141,** 1864–1874 e1861–e1863
6. Barclay, J., Clark, A. K., Ganju, P., Gentry, C., Patel, S., Wotherspoon, G., Buxton, F., Song, C., Ullah, J., Winter, J., Fox, A., Bevan, S., and Malcangio, M. (2007) Role of the cysteine protease cathepsin S in neuropathic hyperalgesia. *Pain* **130,** 225–234
7. Clark, A. K., Yip, P. K., Grist, J., Gentry, C., Staniland, A. A., Marchand, F., Dehvari, M., Wotherspoon, G., Winter, J., Ullah, J., Bevan, S., and Malcangio, M. (2007) Inhibition of spinal microglial cathepsin S for the reversal of neuropathic pain. *Proc. Natl. Acad. Sci. U.S.A.* **104,** 10655–10660
8. Clark, A. K., Yip, P. K., and Malcangio, M. (2009) The liberation of fractalkine in the dorsal horn requires microglial cathepsin S. *J. Neurosci.* **29,** 6945–6954
9. Steinhoff, M., Corvera, C. U., Thoma, M. S., Kong, W., McAlpine, B. E., Caughey, G. H., Ansel, J. C., and Bunnett, N. W. (1999) Proteinase-activated receptor-2 in human skin: tissue distribution and activation of keratinocytes by mast cell tryptase. *Exp. Derm.* **8,** 282–294
10. Steinhoff, M., Vergnolle, N., Young, S. H., Tognetto, M., Amadesi, S., Ennes, H. S., Trevisani, M., Hollenberg, M. D., Wallace, J. L., Caughey, G. H., Mitchell, S. E., Williams, L. M., Geppetti, P., Mayer, E. A., and Bunnett, N. W. (2000) Agonists of proteinase-activated receptor 2 induce inflammation by a neurogenic mechanism. *Nature Med.* **6,** 151–158
11. Ossovskaya, V. S., and Bunnett, N. W. (2004) Protease-activated receptors: contribution to physiology and disease. *Physiol. Rev.* **84,** 579–621
12. Bohm, S. K., Kong, W., Bromme, D., Smeekens, S. P., Anderson, D. C., Connolly, A., Kahn, M., Nelken, N. A., Coughlin, S. R., Payan, D. G., and Bunnett, N. W. (1996) Molecular cloning, expression and potential functions of the human proteinase-activated receptor-2. *Biochem. J.* **314,** 1009–1016
13. Nystedt, S., Emilsson, K., Wahlestedt, C., and Sundelin, J. (1994) Molecular cloning of a potential proteinase activated receptor. *Proc. Natl. Acad. Sci. U.S.A.* **91,** 9208–9212
14. Cottrell, G. S., Amadesi, S., Grady, E. F., and Bunnett, N. W. (2004) Trypsin IV, a novel agonist of protease-activated receptors 2 and 4. *J. Biol. Chem.* **279,** 13532–13539
15. Knecht, W., Cottrell, G. S., Amadesi, S., Mohlin, J., Skåregärde, A., Gedda, K., Peterson, A., Chapman, K., Hollenberg, M. D., Vergnolle, N., and Bunnett, N. W. (2007) Trypsin IV or mesotrypsin and p23 cleave protease-activated receptors 1 and 2 to induce inflammation and hyperalgesia. *J. Biol. Chem.* **282,** 26089–26100
16. Corvera, C. U., Déry, O., McConalogue, K., Böhm, S. K., Khitin, L. M., Caughey, G. H., Payan, D. G., and Bunnett, N. W. (1997) Mast cell tryptase regulates rat colonic myocytes through proteinase-activated receptor 2. *J. Clin. Invest.* **100,** 1383–1393
17. Molino, M., Barnathan, E. S., Numerof, R., Clark, J., Dreyer, M., Cumashi, A., Hoxie, J. A., Schechter, N., Woolkalis, M., and Brass, L. F. (1997) Interactions of mast cell tryptase with thrombin receptors and PAR-2. *J. Biol. Chem.* **272,** 4043–4049
18. Camerer, E., Huang, W., and Coughlin, S. R. (2000) Tissue factor- and factor X-dependent activation of protease-activated receptor 2 by factor VIIa. *Proc. Natl. Acad. Sci. U.S.A.* **97,** 5255–5260
19. Smith, R., Jenkins, A., Lourbakos, A., Thompson, P., Ramakrishnan, V., Tomlinson, J., Deshpande, U., Johnson, D. A., Jones, R., Mackie, E. J., and Pike, R. N. (2000) Evidence for the activation of PAR-2 by the sperm protease, acrosin: expression of the receptor on oocytes. *FEBS letters* **484,** 285–290
20. Hansen, K. K., Sherman, P. M., Cellars, L., Andrade-Gordon, P., Pan, Z., Baruch, A., Wallace, J. L., Hollenberg, M. D., and Vergnolle, N. (2005) A major role for proteolytic activity and proteinase-activated receptor-2 in

the pathogenesis of infectious colitis. *Proc. Natl. Acad. Sci. U.S.A.* **102,** 8363–8368

21. Takeuchi, T., Harris, J. L., Huang, W., Yan, K. W., Coughlin, S. R., and Craik, C. S. (2000) Cellular localization of membrane-type serine protease 1 and identification of protease-activated receptor-2 and single-chain urokinase-type plasminogen activator as substrates. *J. Biol. Chem.* **275,** 26333–26342

22. Wilson, S., Greer, B., Hooper, J., Zijlstra, A., Walker, B., Quigley, J., and Hawthorne, S. (2005) The membrane-anchored serine protease, TM-PRSS2, activates PAR-2 in prostate cancer cells. *Biochem. J.* **388,** 967–972

23. Mize, G. J., Wang, W., and Takayama, T. K. (2008) Prostate-specific kallikreins-2 and -4 enhance the proliferation of DU-145 prostate cancer cells through protease-activated receptors-1 and -2. *Mol. Cancer Res.: MCR* **6,** 1043–1051

24. Oikonomopoulou, K., Hansen, K. K., Saifeddine, M., Tea, I., Blaber, M., Blaber, S. I., Scarisbrick, I., Andrade-Gordon, P., Cottrell, G. S., Bunnett, N. W., Diamandis, E. P., and Hollenberg, M. D. (2006) Proteinase-activated receptors, targets for kallikrein signaling. *J. Biol. Chem.* **281,** 32095–32112

25. Ramsay, A. J., Dong, Y., Hunt, M. L., Linn, M., Samaratunga, H., Clements, J. A., and Hooper, J. D. (2008) Kallikrein-related peptidase 4 (KLK4) initiates intracellular signaling via protease-activated receptors (PARs). KLK4 and PAR-2 are co-expressed during prostate cancer progression. *J. Biol. Chem.* **283,** 12293–12304

26. Ramsay, A. J., Reid, J. C., Adams, M. N., Samaratunga, H., Dong, Y., Clements, J. A., and Hooper, J. D. (2008) Prostatic trypsin-like kallikrein-related peptidases (KLKs) and other prostate-expressed tryptic proteinases as regulators of signalling via proteinase-activated receptors (PARs). *Biol. Chem.* **389,** 653–668

27. Amadesi, S., Nie, J., Vergnolle, N., Cottrell, G. S., Grady, E. F., Trevisani, M., Manni, C., Geppetti, P., McRoberts, J. A., Ennes, H., Davis, J. B., Mayer, E. A., and Bunnett, N. W. (2004) Protease-activated receptor 2 sensitizes the capsaicin receptor transient receptor potential vanilloid receptor 1 to induce hyperalgesia. *J. Neurosci.* **24,** 4300–4312

28. Grant, A. D., Cottrell, G. S., Amadesi, S., Trevisani, M., Nicoletti, P., Materazzi, S., Altier, C., Cenac, N., Zamponi, G. W., Bautista-Cruz, F., Lopez, C. B., Joseph, E. K., Levine, J. D., Liedtke, W., Vanner, S., Vergnolle, N., Geppetti, P., and Bunnett, N. W. (2007) Protease-activated receptor 2 sensitizes the transient receptor potential vanilloid 4 ion channel to cause mechanical hyperalgesia in mice. *J. Physiol.* **578,** 715–733

29. Poole, D. P., Amadesi, S., Veldhuis, N. A., Abogadie, F. C., Lieu, T., Darby, W., Liedtke, W., Lew, M. J., McIntyre, P., and Bunnett, N. W. (2013) Protease-activated receptor 2 (PAR2) protein and transient receptor potential vanilloid 4 (TRPV4) protein coupling is required for sustained inflammatory signaling. *J. Biol. Chem.* **288,** 5790–5802

30. Sipe, W. E., Brierley, S. M., Martin, C. M., Phillis, B. D., Cruz, F. B., Grady, E. F., Liedtke, W., Cohen, D. M., Vanner, S., Blackshaw, L. A., and Bunnett, N. W. (2008) Transient receptor potential vanilloid 4 mediates protease activated receptor 2-induced sensitization of colonic afferent nerves and visceral hyperalgesia. *Am. J. Physiol. Gastrointest. Liver Physiol.* **294,** G1288–G1298

31. Dai, Y., Wang, S., Tominaga, M., Yamamoto, S., Fukuoka, T., Higashi, T., Kobayashi, K., Obata, K., Yamanaka, H., and Noguchi, K. (2007) Sensitization of TRPA1 by PAR2 contributes to the sensation of inflammatory pain. *J. Clin. Invest.* **117,** 1979–1987

32. Vergnolle, N., Bunnett, N. W., Sharkey, K. A., Brussee, V., Compton, S. J., Grady, E. F., Cirino, G., Gerard, N., Basbaum, A. I., Andrade-Gordon, P., Hollenberg, M. D., and Wallace, J. L. (2001) Proteinase-activated receptor-2 and hyperalgesia: A novel pain pathway. *Nature Med.* **7,** 821–826

33. Dulon, S., Cande, C., Bunnett, N. W., Hollenberg, M. D., Chignard, M., and Pidard, D. (2003) Proteinase-activated receptor-2 and human lung epithelial cells: disarming by neutrophil serine proteinases. *Am. J. Resp. Cell Mol. Biol.* **28,** 339–346

34. Ramachandran, R., Mihara, K., Chung, H., Renaux, B., Lau, C. S., Muruve, D. A., DeFea, K. A., Bouvier, M., and Hollenberg, M. D. (2011) Neutrophil elastase acts as a biased agonist for proteinase-activated receptor-2 (PAR2). *J. Biol. Chem.* **286,** 24638–24648

35. Kenakin, T., and Christopoulos, A. (2013) Signalling bias in new drug

36. DeFea, K. A., Zalevsky, J., Thoma, M. S., Déry, O., Mullins, R. D., and Bunnett, N. W. (2000) β-arrestin-dependent endocytosis of proteinase-activated receptor 2 is required for intracellular targeting of activated ERK1/2. *J. Cell Biol.* **148,** 1267–1281

37. Mihara, K., Ramachandran, R., Renaux, B., Saifeddine, M., and Hollenberg, M. D. (2013) Neutrophil Elastase and Proteinase-3 Trigger G Protein-biased Signaling through Proteinase-activated Receptor-1 (PAR1). *J. Biol. Chem.* **288,** 32979–32990

38. Boire, A., Covic, L., Agarwal, A., Jacques, S., Sherifi, S., and Kuliopulos, A. (2005) PAR1 is a matrix metalloprotease-1 receptor that promotes invasion and tumorigenesis of breast cancer cells. *Cell* **120,** 303–313

39. Trivedi, V., Boire, A., Tchernychev, B., Kaneider, N. C., Leger, A. J., O'Callaghan, K., Covic, L., and Kuliopulos, A. (2009) Platelet matrix metalloprotease-1 mediates thrombogenesis by activating PAR1 at a cryptic ligand site. *Cell* **137,** 332–343

40. Austin, K. M., Covic, L., and Kuliopulos, A. (2013) Matrix metalloproteases and PAR1 activation. *Blood* **121,** 431–439

41. Mosnier, L. O., Sinha, R. K., Burnier, L., Bouwens, E. A., and Griffin, J. H. (2012) Biased agonism of protease-activated receptor 1 by activated protein C caused by noncanonical cleavage at Arg46. *Blood* **120,** 5237–5246

42. Schuepbach, R. A., Madon, J., Ender, M., Galli, P., and Riewald, M. (2012) Protease-activated receptor-1 cleaved at R46 mediates cytoprotective effects. *J. Thromb. Haemost.* **10,** 1675–1684

43. Lindner, J. R., Kahn, M. L., Coughlin, S. R., Sambrano, G. R., Schauble, E., Bernstein, D., Foy, D., Hafezi-Moghadam, A., and Ley, K. (2000) Delayed onset of inflammation in protease-activated receptor-2-deficient mice. *J. Immunol.* **165,** 6504–6510

44. Liedtke, W., and Friedman, J. M. (2003) Abnormal osmotic regulation in trpv4-/- mice. *Proc. Natl. Acad. Sci. U.S.A.* **100,** 13698–13703

45. Haerteis, S., Krappitz, M., Bertog, M., Krappitz, A., Baraznenok, V., Henderson, I., Lindström, E., Murphy, J. E., Bunnett, N. W., and Korbmacher, C. (2012) Proteolytic activation of the epithelial sodium channel (ENaC) by the cysteine protease cathepsin-S. *Pflugers Archiv.* **464,** 353–365

46. Dulon, S., Leduc, D., Cottrell, G. S., D'Alayer, J., Hansen, K. K., Bunnett, N. W., Hollenberg, M. D., Pidard, D., and Chignard, M. (2005) *Pseudomonas aeruginosa* elastase disables proteinase-activated receptor 2 in respiratory epithelial cells. *Am. J. Resp. Cell Mol. Biol.* **32,** 411–419

47. Déry, O., Thoma, M. S., Wong, H., Grady, E. F., and Bunnett, N. W. (1999) Trafficking of proteinase-activated receptor-2 and β-arrestin-1 tagged with green fluorescent protein. β-Arrestin-dependent endocytosis of a proteinase receptor. *J. Biol. Chem.* **274,** 18524–18535

48. Jensen, D. D., Godfrey, C. B., Niklas, C., Canals, M., Kocan, M., Poole, D. P., Murphy, J. E., Alemi, F., Cottrell, G. S., Korbmacher, C., Lambert, N. A., Bunnett, N. W., and Corvera, C. U. (2013) The bile acid receptor TGR5 does not interact with beta-arrestins or traffic to endosomes but transmits sustained signals from plasma membrane rafts. *J. Biol. Chem.* **288,** 22942–22960

49. Galés, C., Rebois, R. V., Hogue, M., Trieu, P., Breit, A., Hébert, T. E., and Bouvier, M. (2005) Real-time monitoring of receptor and G-protein interactions in living cells. *Nature Methods* **2,** 177–184

50. Kocan, M., Dalrymple, M. B., Seeber, R. M., Feldman, B. J., and Pfleger, K. D. (2011) Enhanced BRET Technology for the Monitoring of Agonist-Induced and Agonist-Independent Interactions between GPCRs and β-Arrestins. *Frontiers in Endocrinology* **1,** 12

51. Chaplan, S. R., Bach, F. W., Pogrel, J. W., Chung, J. M., and Yaksh, T. L. (1994) Quantitative assessment of tactile allodynia in the rat paw. *J. Neurosci. Methods* **53,** 55–63

52. Vergnolle, N., Cenac, N., Altier, C., Cellars, L., Chapman, K., Zamponi, G. W., Materazzi, S., Nassini, R., Liedtke, W., Cattaruzza, F., Grady, E. F., Geppetti, P., and Bunnett, N. W. (2010) A role for transient receptor potential vanilloid 4 in tonicity-induced neurogenic inflammation. *Br. J. Pharmacol.* **159,** 1161–1173

53. McGuire, J. J., Saifeddine, M., Triggle, C. R., Sun, K., and Hollenberg, M. D. (2004) 2-furoyl-LIGRLO-amide: a potent and selective proteinase-activated receptor 2 agonist. *J. Pharmacology Experimental Therapeutics* **309,** 1124–1131

54. Böhm, S. K., Khitin, L. M., Grady, E. F., Aponte, G., Payan, D. G., and Bunnett, N. W. (1996) Mechanisms of desensitization and resensitization of proteinase-activated receptor-2. *J. Biol. Chem.* **271,** 22003–22016

55. Suen, J. Y., Barry, G. D., Lohman, R. J., Halili, M. A., Cotterell, A. J., Le, G. T., and Fairlie, D. P. (2012) Modulating human proteinase activated receptor 2 with a novel antagonist (GB88) and agonist (GB110). *Br. J. Pharmacol.* **165,** 1413–1423

56. Biniossek, M. L., Nägler, D. K., Becker-Pauly, C., and Schilling, O. (2011) Proteomic identification of protease cleavage sites characterizes prime and non-prime specificity of cysteine cathepsins B, L, and S. *J. Proteome Res.* **10,** 5363–5373

57. Choe, Y., Leonetti, F., Greenbaum, D. C., Lecaille, F., Bogyo, M., Brömme, D., Ellman, J. A., and Craik, C. S. (2006) Substrate profiling of cysteine proteases using a combinatorial peptide library identifies functionally unique specificities. *J. Biol. Chem.* **281,** 12824–12832

58. Elmariah, S. B., Reddy, V. B., and Lerner, E. A. (2014) Cathepsin S Signals via PAR2 and Generates a Novel Tethered Ligand Receptor Agonist. *PloS one* **9,** e99702

59. Ayoub, M. A., and Pin, J. P. (2013) Interaction of Protease-Activated Receptor 2 with G Proteins and β-Arrestin 1 Studied by Bioluminescence Resonance Energy Transfer. *Frontiers in Endocrinology* **4,** 196

60. Lerner, D. J., Chen, M., Tram, T., and Coughlin, S. R. (1996) Agonist recognition by proteinase-activated receptor 2 and thrombin receptor. Importance of extracellular loop interactions for receptor function. *J. Biol. Chem.* **271,** 13943–13947

61. Fan, H. C., Zhang, X., and McNaughton, P. A. (2009) Activation of the TRPV4 ion channel is enhanced by phosphorylation. *J. Biol. Chem.* **284,** 27884–27891

62. Lohman, R. J., Cotterell, A. J., Barry, G. D., Liu, L., Suen, J. Y., Vesey, D. A., and Fairlie, D. P. (2012) An antagonist of human protease activated receptor-2 attenuates PAR2 signaling, macrophage activation, mast cell degranulation, and collagen-induced arthritis in rats. *FASEB J.* **26,** 2877–2887

63. Denadai-Souza, A., Martin, L., de Paula, M. A., de Avellar, M. C., Muscará, M. N., Vergnolle, N., and Cenac, N. (2012) Role of transient receptor potential vanilloid 4 in rat joint inflammation. *Arthritis Rheumatism* **64,** 1848–1858

64. Cenac, N., Andrews, C. N., Holzhausen, M., Chapman, K., Cottrell, G., Andrade-Gordon, P., Steinhoff, M., Barbara, G., Beck, P., Bunnett, N. W., Sharkey, K. A., Ferraz, J. G., Shaffer, E., and Vergnolle, N. (2007) Role for protease activity in visceral pain in irritable bowel syndrome. *J. Clin. Invest.* **117,** 636–647

65. Fichna, J., Mokrowiecka, A., Cygankiewicz, A. I., Zakrzewski, P. K., Malecka-Panas, E., Janecka, A., Krajewska, W. M., and Storr, M. A. (2012) Transient receptor potential vanilloid 4 blockade protects against experimental colitis in mice: a new strategy for inflammatory bowel diseases treatment? *Neurogastro Motility* **24,** e557–e560